J|A|C|S
ARTICLES
Published on Web 09/14/2004

Building Blocks for N-Type Molecular and Polymeric Electronics. Perfluoroalkyl- versus Alkyl-Functionalized Oligothiophenes (nTs; $n = 2-6$). Systematic Synthesis, Spectroscopy, Electrochemistry, and Solid-State Organization

Antonio Facchetti, Myung-Han Yoon, Charlotte L. Stern, Geoffrey R. Hutchison, Mark A. Ratner,* and Tobin J. Marks*

Contribution from the Department of Chemistry and the Materials Research Center, Northwestern University, 2145 Sheridan Road, Evanston, Illinois 60208-3113

Received February 23, 2004; E-mail: ratner@northwestern.edu; t-marks@northwestern.edu

Abstract: The synthesis, comparative physicochemical properties, and solid-state structures of five oligothiophene (nT) series differing in substituent nature and attachment, regiochemistry, and oligothiophene core length (n) are described. These five series include the following 25 compounds: (i) α,ω-diperfluorohexyl-nTs **1** (DFH-nTs, $n = 2-6$), (ii) β,β'-diperfluorohexyl-nTs **2** (isoDFH-nTs, $n = 2-6$), (iii) α,ω-dihexyl-nTs **3** (DH-nTs, $n = 2-6$), (iv) β,β'-dihexyl-nTs **4** (isoDH-nTs, $n = 2-6$), and (v) unsubstituted oligothiophenes **5** (αnTs, $n = 2-6$). All new compounds were characterized by elemental analysis, mass spectrometry, and multinuclear NMR spectroscopy. To probe and address quantitatively how the chemistry and regiochemistry of conjugated core substitution affects molecular and solid-state properties, the entire **1**−**5** series was investigated by differential scanning calorimetry, thermogravimetric analysis, and optical absorption and emission spectroscopies. Single-crystal X-ray diffraction data for several fluorocarbon-substituted oligomers are also presented and compared. The combined analysis of these data indicates that fluorocarbon-substituted nT molecules strongly interact in the condensed state, with unit cell level phase separation between the aromatic core and fluorocarbon chains. Surprisingly, despite these strong intermolecular interactions, high solid-state fluorescence efficiencies are exhibited by the fluorinated derivatives. Insight into the solution molecular geometries and conformational behavior are obtained from analysis of optical and variable-temperature NMR spectra. Finally, cyclic voltammetry data offer a reliable picture of frontier MO energies, which, in combination with DFT computations, provide key information on relationships between oligothiophene substituent effects and electronic response properties.

Introduction

Over the last 10 years, organic-based π-conjugated materials have proven to be important components in the scientific development of new generations of optoelectronic devices,[1] with some applications now reaching commercialization.[2] Among this relatively new class of materials, π-conjugated thiophene-based oligomers (nTs) and polymers (PTs) are central players because of their chemical and electrochemical stability and ready functionalization.[3,4] Besides the classic field of conducting components,[4] these materials are currently under intense investigation for applications in thin film transistors,[5] electroluminescent diodes,[6] lasers,[7] sensors,[8] and photovoltaic cells,[9] as well as fluorescent markers for biomolecules.[10] In addition, new dendritic[11] and crown-annelated[12] molecular structures have recently been described from which it is reasonable to expect new self-assembly modalities, properties, and therefore, materials performance.

(1) (a) Shirakawa, H *Chem. Commun.* **2003**, 1. (b) Karl, N. *Synth. Met.* **2003**, *133*, 649. (c) Dimitrakopoulos, C. D.; Malenfant, P. R. L. *Adv. Mater.* **2002**, *14*, 99. (d) Pron, A.; Rannou, P. *Prog. Polym. Sci.* **2002**, *27*, 135. (e) Katz, H. E.; Bao, Z.; Gilat, S. L. *Acc. Chem. Res.* **2001**, *34*, 359. (f) Crone, B.; Dodabalapur, A.; Llin, Y.-Y.; Filas, R. W.; Bao, Z.; LaDuca, A.; Sarpeshkar, R.; Katz, H. E. *Nature* **2000**, *403*, 521. (g) Tour, J. M. *Acc. Chem. Res.* **2000**, *33*, 791.
(2) (a) *Information Display*; Special OLED issue, June 2003, *19* (6). (b) Tullo, A. H. *Chem. Eng. News* **2000**, *26* (June 26), 20−21. (c) Visit, for instance, the Pioneer Home Page. http://pioneerelectronics.com.
(3) (a) Frere, P.; Raimundo, J.-M.; Blanchard, P.; Delaunay, J.; Richomme, P.; Sauvajol, J.-L.; Orduna, J.; Garin, J.; Roncali, J. *J. Org. Chem.* **2003**, *68*, 5357. (b) Wang, J. Z.; Zheng, Z. H.; Li, H. W.; Huck, W. T. S.; Sirringhaus, H. *Nat. Mater.* **2004**, *3*, 171. (c) Afzali, A.; Breen, T. L.; Kagan, C. R. *Chem. Mater.* **2002**, *14*, 1742.
(4) (a) *Handbook of Oligo- and Polythiophenes*; Fichou, D., Ed.; Wiley-VCH: Weinheim, Germany, 1999. (b) *Polythiophenes: Electrically Conductive Polymers*; Schopf, G., Kossmehl, G.; Eds.; Springer, Berlin, 1997.
(5) (a) Meng, H.; Zheng, J.; Lovinger, A. J.; Wang, B.-C.; Van Patten, P. G.; Bao, Z. *Chem. Mater.* **2003**, *15*, 1778. (b) Mushrush, M.; Facchetti, A.; Lefenfeld, M.; Katz, H. E.; Marks, T. J. *J. Am. Chem. Soc.* **2003**, *125*, 9414.
(6) (a) Pasini, M.; Destri, S.; Porzio, W.; Botta, C.; Giovanella, U *J. Mater. Chem.* **2003**, *13*, 807. (b) Suzuki, M.; Fukuyama, M.; Hori, Y.; Hotta, S. *J. Appl. Phys.* **2002**, *91*, 5706.
(7) (a) Pisignano, D.; Anni, M.; Gigli, G.; Cingolani, R.; Zavelani-Rossi, M.; Lanzani, G.; Barbarella, G.; Favaretto, L. *Appl. Phys. Lett.* **2002**, *81*, 3534.
(8) (a) Torsi, L.; Lovinger, A. J.; Crone, B.; Someya, T.; Dodabalapur, A.; Katz, H. E.; Gelperin, A. *J. Phys. Chem. B* **2002**, *106*, 12563. (b) Roncali, J. *J. Mater. Chem.* **1999**, 9, 1875.
(9) Hara, K.; Kurashige, M.; Dan-Oh, Y.; Kasada, C.; Shinpo, A.; Suga, S.; Sayama, K.; Arakawa, H. *New J. Chem.* **2003**, *27*, 783.
(10) Barbarella, G. *Chemistry* **2002**, *8*, 5072.
(11) Xia, C.; Fan, X.; Loklin, J.; Advincula, R. C. *Org. Lett.* **2002**, *4*, 2067.
(12) Jousselme, B.; Blanchard, P.; Levillain, E.; Delaunay, J.; Allain, M.; Richomme, P.; Rondeau, D.; Gallego-Planas, N.; Roncali, J. *J. Am. Chem. Soc.* **2003**, *125*, 1363.

10.1021/ja048988a CCC: $27.50

Part of the interest in organic (opto)electronics stems from the facile control and flexibility that organic synthetic methodology affords in functionalizing the (oligo, poly)thiophene core. By judicious choice of functionality it is possible to fine-tune key optical, electronic, and electrooptical properties.[13] Electron-donating (alkyl, alkoxy, alkylamino, etc.) or -withdrawing (CHO, CN, NO_2, etc.) substituents can raise or lower the energies of the highest occupied molecular orbital (HOMO) and the lowest unoccupied molecular orbital (LUMO) relative to the unsubstituted system, allowing rational modulation of the molecular "band gap".[14] Appending electron-withdrawing or -donating groups onto the heterocyclic skeleton also alters the redox and optical properties.[14,15] These modifications ultimately affect the charge transport characteristics of the bulk solid and define the role that the material can play in various device configurations.

In the extensive class of functionalized thiophene-based conductors, polythiophenes bearing fluorinated substituents have been barely investigated.[13] For synthetic reasons, most of the structures reported to date feature an "insulating" spacer (alkyl, O, $SiMe_2$) between the fluorinated fragment (usually a perfluoroalkyl group) and the heteroaromatic core, which greatly attenuates or even reverses the electronic effects of fluorocarbon substitution.[16] The only report of a poly(3-perfluoroalkyl)-thiophene is brief mention of the anomalously low oxidation potential of the monomer, 3-trifluoromethylthiophene, compared to the fluoro- and difluoromethyl analogues, and higher oligomers were not described.[17] Leclerc et al.[18] reported the synthesis of regiorandom poly(3′-perfluoroalkyl-2,2′:5′,2″-tertthiophene), which has a higher oxidation potential than the alkyl analogue, but without further details. Very recently, poly(3-perfluorooctyl)-thiophene has been reported and, interestingly, exhibits solubility in supercritical CO_2.[19] However, synthetic details and polymer molecular weight have not been disclosed. As far as oligothiophenes are concerned, to the best of our knowledge, no systematic study has been reported concerning homologous series of fluorocarbon-substituted oligothiophenes with well-defined substitution patterns, chain, and π-core lengths. This is a clear deficiency since oligothiophenes have been shown to be viable models for predicting and understanding the electronic structures and optical properties of the corresponding polymers. Furthermore, the limited literature concerning (semi)-fluorinated (oligo, poly)heteroaromatic conductors stands in sharp contrast to other classes of organic compounds where the unique (per)fluorination-related properties such as high chemical and biological stability, volatility, thermal stability, low coefficient of friction, hydro- and lipophobicity, and permeability to some gases have afforded diverse applications in materials and medicinal chemistry and in biochemistry.[20] It is therefore expected that incorporation of the aforementioned properties into π-conjugated conductors will lead to novel materials of potential fundamental scientific and technological interest.

In a recent communication,[21] we described a limited number of the first end-capped fluorocarbon-functionalized oligothiophenes and reported on the consequences of fluorine-for-hydrogen substitution on the molecular and thin-film semiconductor properties. That preliminary report revealed unexpected similarities, differences, and trends within and between fluoroalkyl- and the corresponding, widely investigated, alkyl-functionalized nTs and raised a number of intriguing questions. The present contribution describes a complete account of our studies aimed at better fundamental understanding of the chemical, structural, and physical properties as well as solid-state characteristics of five homologous series of thiophene-based π-conjugated materials. The questions we address are whether other classes of fluorocarbon-substituted oligothiophenes are synthetically accessible, how the properties of fluorocarbon-substituted oligothiophenes correlate with those of the other classes of fluorine-free nTs, whether a straightforward model can explain the trends found, and whether potential applications exist in the large field of π-electron organic solids. To achieve these goals, a full series of compounds has been synthesized and investigated, ranging from the α,ω-diperfluorohexyl-substituted series **1** (DFH-nTs, $n = 2-6$) and the corresponding α,ω-dihexyl-substituted system **3** (DH-nTs, $n = 2-6$) to the parent unsubstituted oligothiophenes **5** (αnTs, $n = 2-6$). In addition, to fully address regiochemistry effects, isomerically pure β,β'-diperfluorohexyl-substituted series **2** (isoDFH-nTs, $n = 2-6$) has been synthesized for the first time and is compared to the β,β'-dihexyl-functionalized system **4** (isoDH-nTs, $n = 2-6$). These latter systems provide additional insights into the molecular and solid-state properties of fluoroalkyl- versus alkyl-oligothiophenes functionalized at a different skeletal position. Also, since the α,ω-positions are free, they provide key building blocks for the preparation of, and are probably better descriptors of, the properties of the corresponding regioregular fluorinated polymers. In addition to the aformentioned syntheses, the molecular properties of these homologous and homogeneous sets of compounds are compared and contrasted in detail by a combination of techniques, including differential scanning calorimetry (DSC) and thermogravimetric analysis (TGA), optical absorption (UV−vis), emission (PL) spectroscopies, multinuclear NMR spectroscopy, and cyclic voltammetry (CV). Single-crystal XRD data are obtained for key members of the fluorinated family, and density-functional theory (DFT) modeling provides additional insights into experimental results. Finally, thin films are grown on glass substrates and studied by UV−vis and PL spectroscopy. With full understanding of **1**−**5** molecular physical properties and

(13) (a) *Electronic Materials: The Oligomer Approach*; Müllen, K., Wegner, G. Eds.; Wiley-VCH: New York, 1998. (b) *Handbook of Conductive Polymers*; Skotheim, T. A., Elsenbaumer R. L., Reynolds, J. R., Eds.; Marcel Dekker: New York, 1998; pp 325−326.
(14) (a) Casado, J.; Pappenfus, T. M.; Miller, L. L.; Mann, K. R.; Orti, E.; Viruela, P. M.; Pou-Amerigo, R.; Hernandez, V.; Lopez Navarrete, J. T. *J. Am. Chem. Soc.* **2003**, *125*, 2524. (b) Moratti, S. C.; Cervini, R.; Holmes, A. B.; Baigent, D. R.; Friend, R. H.; Greenham, N. C.; Grüner, J.; Hamer, P. J. *Synth. Met.* **1995**, *71*, 2117.
(15) (a) Casado, J.; Miller, L. L.; Mann, K. R.; Pappenfus, T. M.; Higuchi, H.; Orti, E.; Milian, B.; Pou-Amerigo, R.; Hernandez, V.; Lopez Navarrete, J. T. *J. Am. Chem. Soc.* **2002**, *124*, 12380. (b) Lux, A.; Holmes, A. B.; Cervini, R.; Davies, J. E.; Moratti, S. C.; Grüner, J.; Cacialli, F.; Friend, R. H. *Synth. Met.* **1997**, *84*, 293. (c) Brédas, J. *Adv. Mater.* **1995**, *7*, 263.
(16) (a) Collard, D. M.; Li, L.; Hong, X. M. *Polym. Mater. Sci. Eng.* **2002**, *86*, 38. (b) Laforgue, A.; Simon, P.; Fauvarque, J.-F. *Synth. Met.* **2001**, *123*, 311. (c) Hong, X. M.; Collard, D. M. *Macromolecules* **2000**, *33*, 3502. (d) Hong, X. M.; Tyson, J. C.; Collard, D. M. *Macromolecules* **2000**, *33*, 6916. (e) Thobie-Gautier, C.; Guy, A.; Gougues, A.; Jubault, M.; Roncali, J. *Adv. Mater.* **1993**, *5*, 637. (f) Kassmi, A. E.; Buchner, W.; Fache, F.; Lemaire, M. *J. Electroanal. Chem.* **1992**, *326*, 357. (g) Buchner, W.; Garreau, R.; Lemaire, M.; Roncali, J.; Garnier, F. *J. Electroanal. Chem.* **1990**, *277*, 355.
(17) Ritter, S. K.; Noftle, R. E.; Ward, A. E. *Chem. Mater.* **1993**, *5*, 752.
(18) Robitaille, L.; Leclerc, M. *Macromolecules* **1994**, *27*, 1847.
(19) Li, L.; Counts, K. E.; Kurosawa, S.; Teja, A. S.; Collard, D. M. *Adv. Mater.* **2004**, *16*, 180.
(20) Hiyama, T. *Organofluorine Compounds: Chemistry and Applications*; Springer-Verlag: Berlin, 2000.
(21) Facchetti, A.; Mushrush, M.; Katz, H. E.; Marks, T. J. *Adv. Mater.* **2003**, *15*, 33.

Chart 1

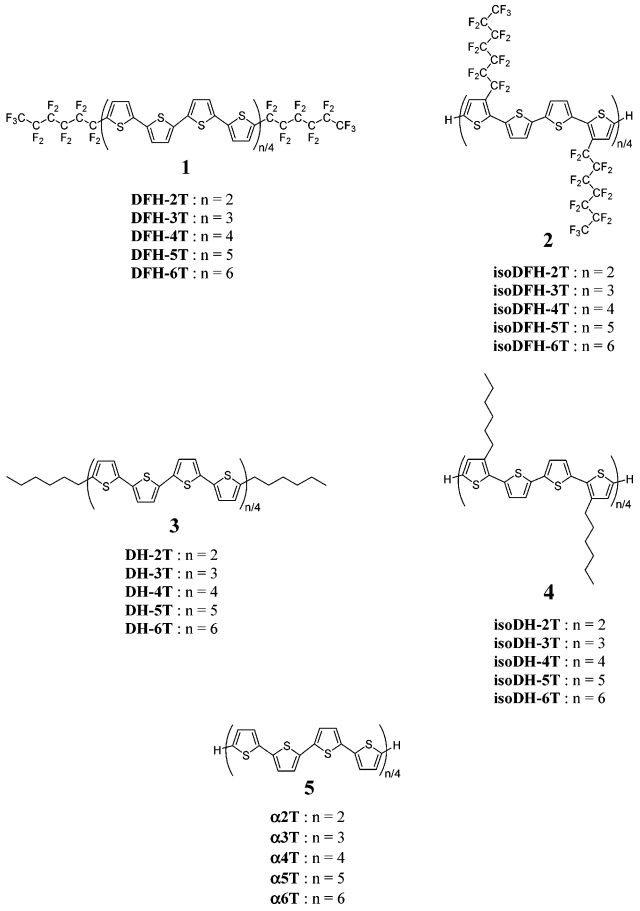

knowledge of single-crystal geometries and organization, the next goal is to provide additional insights into solid-state microstructure and define a field of potential application as a new class of materials. In a related contribution,[22] we describe thin film growth and microstructure properties and morphologies of the present compounds, and electrical response in field-effect transistor (FET) device configurations. The combined results provide key and surprising information on the properties and solid-state organization of fluoroalkyl-containing oligothiophenes, and a coherent picture of how these properties correlate with those of the fluorine-free analogues. Chart 1 shows the structures of **1**−**5**.

Experimental Section

The following compounds were prepared according to known procedures:[23] 5,5‴″-diperfluorohexyl-2,2′:5′,2″:5″,2‴:5‴,2⁗:5⁗,2⁗′-sexithiophene (**DFH-6T**),[23a] 5,5′-dihexyl-2,2′-dithiophene (**DH-2T**),[23b] 5,5′-dihexyl-2,2′:5′,2″-terthiophene (**DH-3T**),[23c] 5,5‴-dihexyl-2,2′:5′,2″:5″,2‴-quaterthiophene (**DH-4T**),[23d] 5,5⁗′-dihexyl-2,2′:5′,2″:5″,2‴:5‴,2⁗:5⁗,2⁗′-quinquethiophene (**DH-5T**),[23e] 5,5⁗′-dihexyl-2,2′:5′,2″:5″,2‴:5‴,2⁗:5⁗,2⁗′:5⁗′,2⁗″-sexithiophene (**DH-6T**),[23f] 2,2′:5′,2″:5″,2‴-quaterthiophene (**α4T**),[23g] 2,2′:5′,2″:5″,2‴:5‴,2⁗:5⁗,2⁗′-quinquethiophene (**α5T**),[23h] 2,2′:5′,2″:5″,2‴:5‴,2⁗:5⁗,2⁗′:5⁗′,2⁗″-sexithiophene (**α6T**),[23i] 5,5′-dibromo-2,2′-bithiophene (**6**),[23j] 2-(1-perfluorohexyl)thiophene (**7**),[23k] 5-perfluorohexyl-5′-bromo-2,2′-dithiophene (**10**),[23a] 5-bromo-2,2′-bithiophene (**12**),[23l] 2,5-bis(tri-*n*-butylstannyl)thiophene (**13**), 5,5′-bis(tri-*n*-butylstannyl)-2,2′-dithiophene (**14**),[23m] 5-bromo-2,2′:5′,2″-terthiophene (**15**),[23n] 3,3′,5,5′-tertrabromo-2,2′-bithiophene (**17**),[23o] 3,3′-dibromo-2,2′-bithiophene (**18**),[23o] 3-bromo-2,2′-bithiophene (**22**).[23n]

The following are new compounds. For synthetic characterization and computational details as well as film growth methods, see Supporting Information.

5,5′-Diperfluorohexyl-2,2′-dithiophene (**DFH-2T**). mp 97 °C. Anal. Calcd for $C_{20}H_4F_{26}S_2$: C, 29.94; H, 0.50; F, 61.57. Found: C, 29.90; H, 0.57; F, 61.73. HRMS (EI, 70 eV): found *m*/*z*, 801.9336 (M^+), calcd for $C_{20}H_4F_{26}S_2$, 801.9334. *5,5′-Diperfluorohexyl-2,2′:5′,2″-terthiophene* (**DFH-3T**). mp 132 °C. Anal. Calcd for $C_{24}H_6F_{26}S_3$: C, 32.59; H, 0.685; F, 55.85. Found: C, 32.50; H, 0.69; F, 55.63. HRMS (EI, 70 eV): found *m*/*z*, 883.9226 (M^+), calcd for $C_{24}H_6F_{26}S_3$, 883.9217. *5,5‴-Diperfluorohexyl-2,2′:5′,2″:5″,2‴-quaterthiophene* (**DFH-4T**). mp 213 °C. Anal. Calcd for $C_{28}H_8F_{26}S_4$: C, 34.81; H, 0.84; F, 51.14. Found: C, 34.66; H, 0.94; F, 51.06; MS (EI, 70 eV), 965.9 (M^+, 100%). *5,5⁗′-Diperfluorohexyl-2,2′:5′,2″:5″,2‴:5‴,2⁗:5⁗,2⁗′-quinquethiophene* (**DFH-5T**). mp 252 °C. Anal. Calcd for $C_{32}H_{10}F_{26}S_5$: C, 36.64; H, 0.96; F, 47.10. Found: C, 36.71; H, 1.12; F, 47.49. *3,3′-Diperfluorohexyl-2,2′-dithiophene* (**isoDFH-2T**). Oil. HRMS (EI, 70 eV): found *m*/*z*, 801.9362, calcd for $C_{14}H_5F_{13}S_2$ (M^+), 801.9339. *3,3″-Diperfluorohexyl-2,2′:5′,2″-terthiophene* (**isoDFH-3T**). HRMS (EI, 70 eV): found *m*/*z*, calcd for $C_{24}H_6F_{26}S_3$ (M^+). *3,3‴-Diperfluorohexyl-2,2′:5′,2″:5″,2‴-quaterthiophene* (**isoDFH-4T**). mp 145 °C. Anal. Calcd for $C_{28}H_8F_{26}S_4$: C, 34.79; H, 0.83; F, 51.10. Found: C, 34.85; H, 0.95; F, 51.05. *3,3⁗′-Diperfluorohexyl-2,2′:5′,2″:5″,2‴:5‴,2⁗:5⁗,2⁗′-quinquethiophene* (**isoDFH-5T**). mp 160 °C. Anal. Calcd for $C_{32}H_{10}F_{26}S_5$: C, 33.65; H, 0.76; F, 47.10. Found: C, 36.64; H, 1.17; F, 47.38. *3,3⁗″-Diperfluorohexyl-2,2′:5′,2″:5″,2‴:5‴,2⁗:5⁗,2⁗′:5⁗′,2⁗″-sexithiophene* (**isoDFH-6T**). mp 217 °C. Anal. Calcd for $C_{36}H_{12}F_{26}S_6$: C, 38.24; H, 1.07; F, 43.69. Found: C, 38.41; H, 1.07; F, 43.60. *3,3⁗″-Dihexyl-2,2′:5′,2″:5″,2‴:5‴,2⁗:5⁗,2⁗′-qinquethiophene* (**iso-DH-5T**). mp 77−78 °C (hexane). HRMS (EI, 70 eV): found *m*/*z*, 580.1415 (M^+), calcd for $C_{32}H_{36}S_5$, 580.1410. Anal. Calcd for $C_{32}H_{36}S_5$: C, 6616; H, 6.26. Found: C, 65.98; H, 5.96. *3,3⁗″-Hexyl-2,2′:5′,2″:5″,2‴:5‴,2⁗:5⁗,2⁗′:5⁗′,2⁗″-sexithiophene* (**isoDH-6T**). mp 137 °C (toluene-hexane). Anal. Calcd for $C_{36}H_{38}S_6$: C, 65.21; H, 5.78. Found: C, 65.40; H, 5.59.

2-(Tri-n-butylstannyl)-5-(1-perfluorohexyl)thiophene (**8**). Oil. HRMS/EI (70 eV) Calcd for $C_{22}H_{29}SSnF_{13}$: 692.0804, found: 692.0729 (M^+). *5-Perfluorohexyl-2,2′-dithiophene* (**9**). mp 51 °C. Anal. Calcd for $C_{14}H_5F_{13}S_2$: C, 34.72; H, 1.04; F, 51.00. *5-(tri-n-Butylstannyl)-5′-(1-perfluorohexyl)-2,2′-dithiophene* (**11**). Oil. HRMS (EI, 70 eV): found *m*/*z*, 774.0680, calcd for $C_{26}H_{44}S_2Sn$ (M^+), 774.0682. *5-Perfluorohexyl-2,2′:5′,2″-terthiophene* (**17**). mp 158 °C (*i*-PrOH). Anal. Calcd for $C_{18}H_7F_{13}S_3$: C, 38.17; H, 1.25; F, 43.61. Found: C, 37.95; H, 1.18; F, 44.01. HRMS (EI, 70 eV): found *m*/*z*, 565.9501, calcd for $C_{18}H_7F_{13}S_3$ (M^+), 565.9502. *3,3′,5,5′-Tetrabromo-2,2′:5′,2″-terthiophene* (**19**). mp 156 °C (toluene). Anal. Calcd for $C_{12}H_4Br_4S_3$: C, 25.56; H, 0.72. Found: C, 25.08; H, 0.82. *3,3′-Dibromo-2,2′:5′,2″-terthiophene* (**20**). mp 106 °C. Anal. Calcd for $C_{12}H_6Br_2S_3$: C, 35.48; H, 1.49. Found: C, 35.22; H, 1.48. *3-Perfluorohexyl-2,2′-dithiophene* (**23**). Oil. Anal. Calcd for $C_{14}H_5F_{13}S_2$: C, 34.72; H, 1.04; F, 51.00. Found: C, 35.01;

(22) Facchetti, A.; Mushrush, M.; Yoon, M.-H.; Hutchison, G. R.; Ratner, M. A.; Marks, T. J. *J. Am. Chem. Soc.*, in press.

(23) (a) Facchetti, A.; Deng, Y.; Wang, A.; Koide, Y.; Sirringhaus, H.; Marks, T. J.; Friend, R. H. *Angew. Chem., Int. Ed.* **2000**, *39*, 4547. (b) Barbarella, G.; Favaretto, G.; Sotgiu, G.; Zambianchi, L.; Pudova, O.; Bongini, A. *J. Org. Chem.* **1998**, *63*, 5497. (c) Byron, D.; Matharu, A.; Wilson, R.; Wright, G. *Mol. Cryst. Liq. Cryst. Sci. Technol., Sect. A* **1995**, *265*, 61. (d) Garnier, F.; Hajlaoui, R.; El Kassmi, A.; Horowitz, G.; Laigre, L.; Porzio, W.; Armanini, M.; Provasoli, F. *Chem. Mater.* **1998**, *10*, 3334. (e) Li, W.; Katz, H. E.; Lovinger, A. J.; Laquindanum, J. G. *Chem. Mater.* **1999**, *11*, 458. (f) Garnier, F.; Yassar, A.; Hajlaoui, R.; Horowitz, G.; Deloffre, F.; Servet, B.; Ries, S.; Alnot, P. *J. Am. Chem. Soc.* **1993**, *115*, 8716. (g) Kagan, J.; Arora, S. K. *Heterocycles* **1983**, *20*, 1937. (h) Nakayama, J.; Nakamura, Y.; Murabayashi, S.; Hoshino, M. *Heterocycles* **1987**, *26*, 939. (i) Katz, H. E.; Torsi, L.; Dodabalapur, A. *Chem. Mater.* **1995**, *7*, 2235. (j) Nenajdenko, V. G.; Baraznenok, I. L.; Balenkova, E. S. *J. Org. Chem.* **1998**, *63*, 6132. (k) Chen, G. J.; Tamborski, J. *Fluorine Chem.* **1990**, *46*, 137. (l) Bauerle, P.; Wurthner, F.; Gotz, G.; Effenberger, F. *Synthesis* **1993**, *11*, 1099. (m) Wei, Y.; Yang, Y.; Yeh, J.-M. *Chem. Mater.* **1996**, *8*, 2659. (n) Nakayama, J.; Konishi, T.; Murabayashi, S.; Hoshino, M. *Heterocycles* **1987**, *26*, 1793. (o) Yu, W.-L.; Meng, H.; Pei, J.; Huang, W.; Li, Y.; Heeger, A. J. *Macromolecules* **1998**, *31*, 4838.

Scheme 1. Synthesis of Compounds of Family **1**[a]

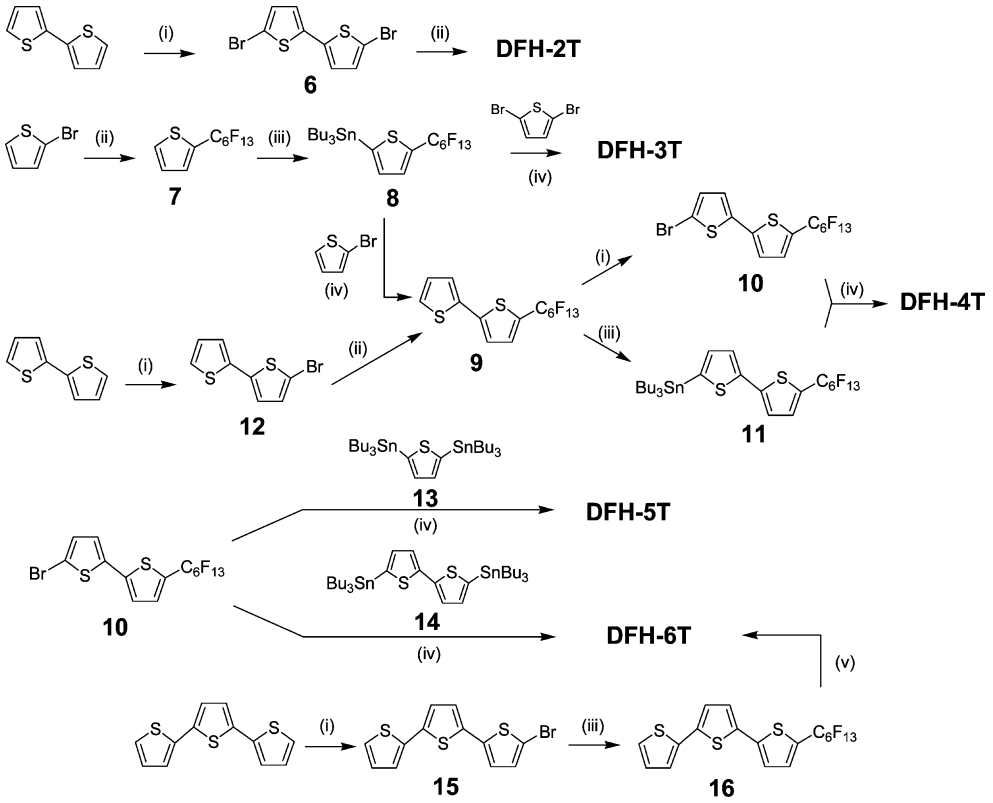

[a] (i) NBS; (ii) Cu bronze, $C_6F_{13}I$; (iii) BuLi, Bu_3SnCl; (iv) $Pd(PPh_3)_4$; and (v) BuLi, $CuCl_2$.

H, 1.04; F, 49.98. *5,5‴-Bis-trimethylsilyl-3,3‴-diperfluorohexyl-2,2′:5′,2″:5″,2‴-quaterthiophene* (**25**). mp 173 °C. Anal. Calcd for $C_{34}H_{24}F_{26}S_4Si_2$: C, 36.75; H, 2.18; F, 44.46. Found: C, 36.67; H, 2.18; F, 44.76. *3-(1-Perfluorohexyl)-5′-bromo-2,2′-dithiophene* (**27**). Oil. HRMS (EI, 70 eV): found *m/z*, 563.8721, calcd for $C_{14}H_4BrF_{13}S_2$ (M^+), 563.8709. *3-Hexyl-5′-bromo-2,2′-dithiophene* (**28**). Oil. HRMS (EI, 70 eV): found *m/z*, 327.9942, calcd for $C_{14}H_{17}BrS_2$ (M^+), 327.9955.

Results

Synthesis. In contrast to alkylation reactions,[24] there are relatively few convenient synthetic methods for introducing perfluoroalkyl groups on aromatic and heteroaromatic skeletons. Among them are copper-promoted coupling reactions between perfluoroalkyl iodides and aromatic halides,[25a,b] $(Ph_3P)_3RuCl_2$-catalyzed[25c] or photoinduced[25d,e] reactions of perfluoroalkanesulfonyl halides with aromatic halides, and sulfinatodehalogenation.[25f,g] The synthetic route chosen here involves coupling of perfluorohexylcuprate (from perfluorohexyl iodide and copper bronze) with the appropriate bromothiophene derivative in DMSO. Extension of the thiophene(s) core from two to six thiophene units is accomplished principally via Pd(0)-catalyzed coupling of bromothiophene derivatives with stannyl (Stille coupling)[26a] and Grignard (Kumada coupling)[26b] thienyl reagents.

End-capped fluoroalkyl compounds DFH-nTs (**1**) were prepared according to Scheme 1. The shortest oligomer **DFH-2T** was prepared without thienyl−thienyl coupling, but directly via perfluoroalkylation of dibromodithiophene **6** in ∼40% yield. This yield is somewhat lower compared to similar reactions on monobrominated systems (50−80%) and probably reflects the large molar excess of perfluorohexyl iodide employed. Such a ratio avoids formation of monofluorinated derivatives from which **DFH-2T** is difficult to separate. For the synthesis of the other DFH-nTs, the final step involves a Stille coupling reaction, which proceeds in yields greater than 80%. An attempt to prepare **DFH-6T** by Cu(II)-promoted dimerization of lithiated terthiophene **16** affords impure samples in low yield. The ^1H NMR spectrum of a portion quenched with D_2O indicates formation of 5″-lithum-5-bromotertthiophene in the presence of other lithiated species. Dimerization of this mixture results inevitably in formation of a variety of products. All of the longer oligomers prepared via Stille coupling can be purified by gradient sublimation. The optimization of key intermediate **9**, which affords **10** upon bromination, was performed. This system was initially prepared in 42% overall yield, starting from dithiophene.[23a] Major problems encountered are the difficult isolation of **12** in good yield from dibrominated **6** and separation of **9** from other fluorinated products. For this reason, a more efficient route starts from commercially available 2-bromothiophene, which can be converted to **7** in excellent yield and easily purified by distillation. Quantitative metalation of **7**

(24) March, J. *Advanced Organic Chemistry: Reactions, Mechanisms, and Structure*; Wiley: New York, 1992.

(25) (a) Chen, G. J.; Tamborski, C. *J. Fluorine Chem.* **1990**, *46*, 137. (b) Mcloughlin V. C. R.; Thrower, J. *Tetrahedron* **1969**, *25*, 5921. (c) Kamigata, N.; Yoshikawa, M.; Shimizu, T. *J. Fluorine Chem.* **1998**, *87*, 91. (d) Nakamura, T.; Koga, Y. *J. Chem. Soc., Perkin Trans. 2* **1998**, *3*, 659. (e) Dolbier, W. R. *Chem. Rev.* **1996**, *96*, 1557. (f) Huang, X.-T.; Long, Z.-Y.; Chen, Q.-Y. *J. Fluorine Chem.* **2001**, *111*, 107. (g) Huang, W.-Y.; Wu, F.-H. *Israel J. Chem.* **1999**, *39*, 167.

(26) (a) Stille, K. J. *Angew. Chem., Int. Ed. Engl.* **1986**, *25*, 508. (b) Tamao, K. *J. Organomet. Chem.* **2002**, *653*, 23. (c) Kumada, M. *Pure Appl. Chem.* **1980**, *52*, 669.

Scheme 2. Synthesis of Compounds of Family **2**[a]

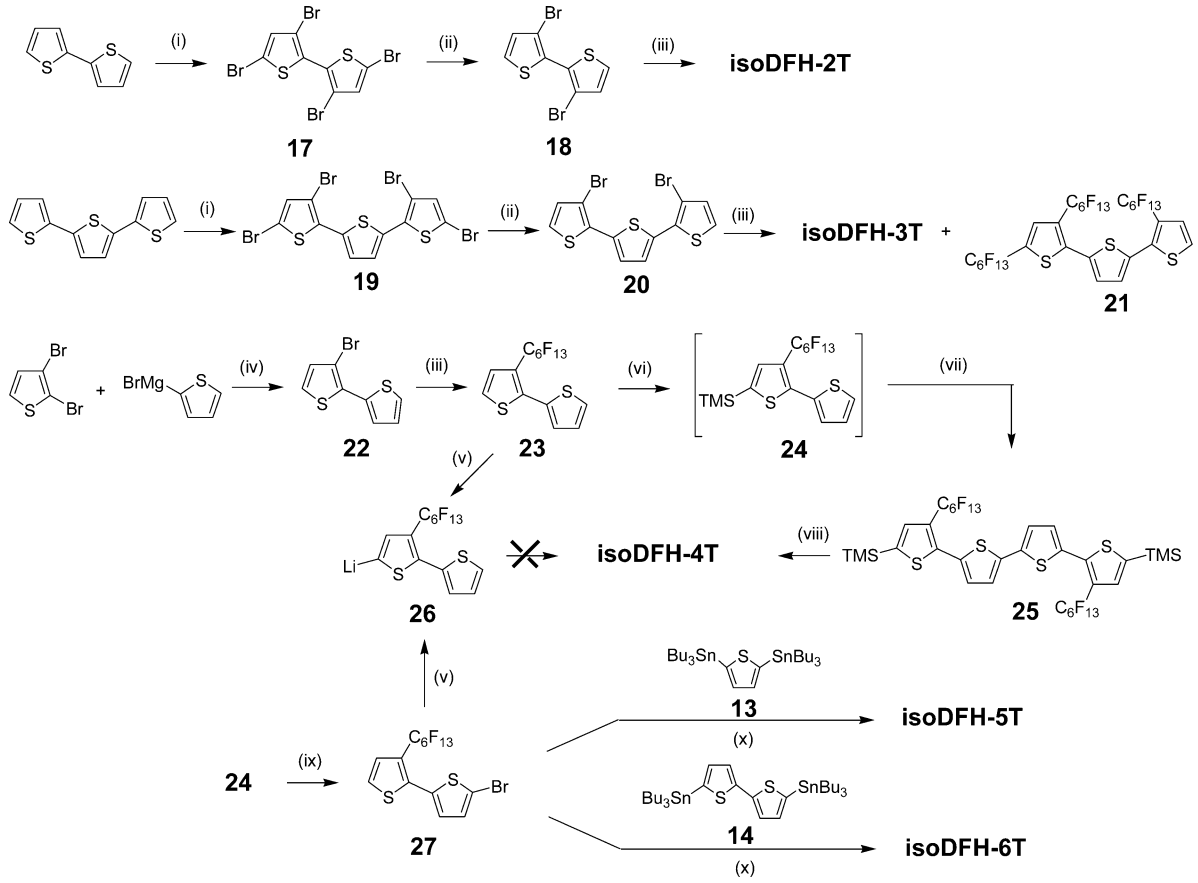

[a] (i) Br_2; (ii) Zn + HCl; (iii) Cu bronze, $C_6F_{13}I$; (iv) $PdCl_2$dppf; (v) BuLi; (vi) BuLi, TMSCl; (vii) BuLi, $CuCl_2$; (viii) CF_3SO_3H; (ix) NBS; and (x) $Pd(PPh_3)_4$.

affords stannyl derivative **8**, which reacts with 2-bromothiophene to afford **9** in >70% overall yield.

The synthetic routes to regioisomeric isoDFH-nTs (**2**) are summarized in Scheme 2. The shortest oligomers, **isoDFH-2T** and **isoDFH-3T**, were prepared following the same synthetic route starting from di- and terthiophene, respectively, which were regioselectively perbrominated at the 3- and 5-positions of the external rings to yield **17** and **19**. This reaction has never been attempted with **α3T**, and it is remarkable that the central thiophene ring does not undergo electrophilic attack by Br_2. Removal of the terminal bromo substituents of **17** and **19** was achieved with Zn powder in HCl-EtOH to afford dibromo derivatives **18** and **20**, respectively, in excellent yields. Perfluoroalkylation of the latter compounds affords, after column chromatography, **isoDFH-2T** and **isoDFH-3T**, respectively, in modest yields (~40%) due to the formation of large quantities of byproducts. One of these byproducts, triperfluoroalkyl-3T **21**, was isolated in moderate yield (27%). The key intermediate for the synthesis of **isoDFH-4T** is 3-perfluorohexyldithiophene (**23**), which is conveniently prepared from parent compound **22**. Since the reaction of **23** with *n*-BuLi affords 5-lithium-3-perfluorohexyl-2,2′-dithiophene (**26**), direct dimerization of the latter to give **isoDFH-4T** is not feasible. Note also that reaction between bromodithiophene **27** and *n*-BuLi affords **26**, clearly indicating that prefluoroalkyl functionalization substantially increases the thiophene ring acidity. Therefore, to achieve regiochemically correct coupling, compound **23** was lithiated and quenched with TMSCl. Intermediate **24** (obtained in >95% yield by ^{1}H NMR analysis) was not isolated but lithiated again and dimerized with $CuCl_2$ to afford bisTMS-quaterthiophene **25** in 52% yield. In the last step, the TMS groups of **25** were removed with CF_3SO_3H, providing **isoDFH-4T** quantitatively. The longest oligomers, **isoDFH-5T** and **isoDFH-6T**, were obtained in ~80% yields by reaction of **27** with bistributylstannyl derivatives **13** and **14**, respectively.

Finally, the novel, regiochemically pure β,β'-dialkyl substituted oligothiophenes isoDH-nTs (n = 5, 6) were prepared according to Scheme 3. The key intermediate, bromo derivative **28**, is unknown and was conveniently prepared via Ni(II)-catalyzed reaction of the Grignard reagents of 2-bromo-3-hexylthiophene and 2,5-dibromothiophene in good yield. Bromination of parent compound **29** with either Br_2 or NBS affords a mixture of two bromodithiophenes, **28** and **29**, inseparable by conventional methods. Isomer **29** is formed in surprisingly high selectivity (~70%), in agreement with observations of Bäuerle et al.[27] for 3-dodecyl-2,2′-dithiophene bromination. The target compounds **isoDH-5T** and **isoDH-6T** were obtained via Stille coupling of pure **28** with **13** and **14**, respectively, and isolated in ~80% yields.

Multinuclear NMR Spectroscopy and Rotational Barriers. ^{1}H and ^{19}F NMR spectra were recorded to confirm the molecular structures and purity of the novel, fluorine-containing DFH-nTs (**1**) and isoDFH-nTs (**2**) systems. ^{1}H NMR spectra of **1** and **2** exhibit, compared to the corresponding fluorine-free DH-

(27) Bäuerle, P.; Pfau, F.; Schlupp, H.; Wuerthner, F.; Gaudl, K. U.; Balparda Caro, M.; Fischer, P. *J. Chem. Soc., Perkin Trans. 2* **1993**, *3*, 489.

Scheme 3. Synthesis of Novel Compounds of Family **4**[a]

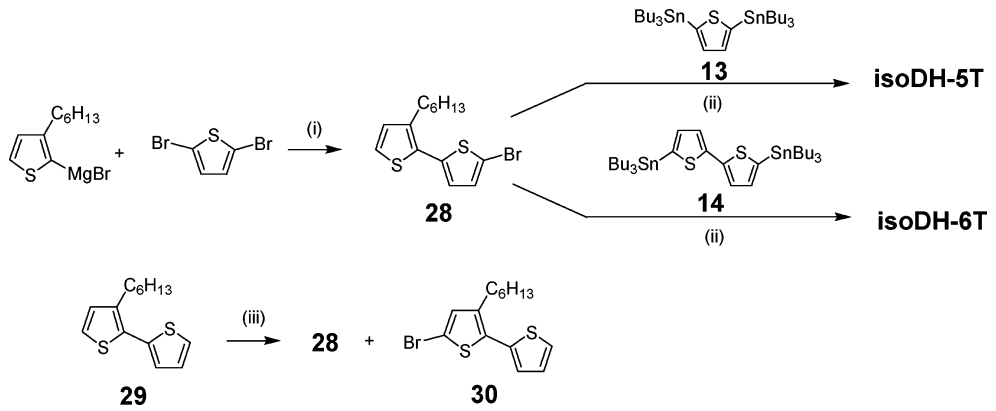

[a] (i) $PdCl_2$dppf; (ii) $Pd(PPh_3)_4$; and (iii) NBS or Br_2.

nT (**3**) and isoDH-nT (**4**) analogues, low-field displacements of the aromatic proton(s) adjacent to the perfluorohexyl chain. As an example, Figure S1A (Supporting Information) shows ^{1}H NMR spectra of **DFH-5T** and **DH-5T**. This result is the first indication that strong σ-electron-withdrawing (-*I*) fluorocarbon substitution decreases thiophene electron density, which correlates with a shift of the proton resonances toward low fields.[28] At room temperature, the ^{19}F NMR spectra of DFH-nTs ($n = 2-6$) and isoDH-nTs ($n = 3-6$) exhibit the usual pattern of an aromatic-bonded C_6F_{13} group, with the appropriate number of ^{19}F resonances (Figure S1B). In contrast, the ^{19}F NMR spectra of **isoDFH-2T** and **isoDFH-3T** are more complex. Particularly interesting is the spectrum of the former compound, which exhibits patterns in which the α- and β-CF_2 signals appear as AX systems, indicating the presence of a stereogenic center (see 20 °C spectrum in Figure 1A). Thus, at room temperature, the ground-state molecular conformation(s) render the fluorines of the α- and β-CF_2 groups diastereotopic. Since this phenomenon has never previously been observed for alkyl-substituted oligothiophenes (vide infra), it was additionally investigated by variable-temperature NMR spectroscopy (Figure 1A). On cooling from +20 to − 60 °C, additional CF_2 resonances of the γ- and δ-CF_2 appear as AB systems. These strongly coupled doublets have geminal F−F coupling constant that increase on moving away from the thiophene core [J_{F-F} (Hz): αα′ (276) < $\beta\beta'$ (299) < $\gamma\gamma'$ (301) < $\delta\delta'$ (307)]. A similar increase in J_{F-F} going from the α- to the terminal CF_2 was observed by Hughes et al. for fluoroalkyl complexes of (TMEDA)Pd(II).[29] As the temperature is raised from +20 to +130 °C, pairwise coalescence of the diastereotopic resonances is observed, which occurs at ∼+70 °C for the β-CF_2 signals and at ∼+105 °C for α-CF_2 signals.

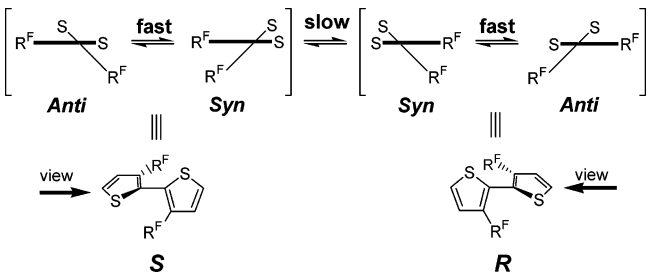

The origin of **isoDFH-2T** chirality lies in the noncoplanarity of the bithiophene core and the relatively large barrier for conformational interchange (slow exchange on the ^{19}F NMR time scale) between *R* and *S* enantiomers. Note that each of these systems might represent a fast interconversion (on the NMR time scale) of *syn* and *anti* conformers. However, we will demonstrate that this is not the case (see Discussion). Several theoretical and experimental studies of oligo- and polythiophene conformations have been reported.[30a−d] The theoretical analyses have consistently indicated that *syn* and *anti* conformers are nonplanar. The energies, and thus populations, of these conformers are comparable, and their interconversion barriers are very small (1−2 kcal/mol). A recent experimental study by Holdcroft et al. also indicates that the barriers to conformational interchange in oligothiophenes are too low to be measured by dynamic NMR spectroscopy,[30e] contrasting previous investiga-

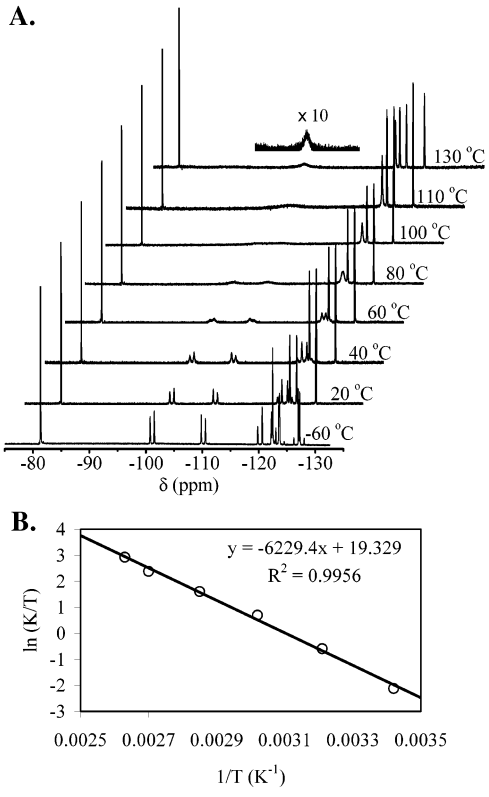

Figure 1. (A) ^{19}F NMR spectra of **isoDFH-2T** in toluene-d_8 as a function of temperature. The spectrum at 130 °C was obtained in $C_2D_2Cl_4$. (B) Corresponding Eyring plot for the exchange process involving the α-CF_2 group.

tions on alkyl-substituted tert- and quaterthiophenes where barriers in the range of 8−20 kcal/mol were reported.[30f,g] The former study[30e] also investigated **isoDH-2T** and concluded that even at temperatures as low as −130 °C, the NMR spectrum is consistent with the presence of a conformationally averaged system.

For the above reasons and the contradictory results reported on the alkyl-substituted compounds, **isoDH-2T** was investigated again in the temperature range of −60 to +130 °C. Our results are in agreement with those of Holdcroft et al., and the conformational interconversion barrier could not be obtained for any of the other isoDH-nTs (n = 3−6) via NMR. On the other hand, the gNMR full shape analysis program could be used to calculate the activation energies of *R*- and *S*-**isoDFH-2T** enantiomer interconversion. The geminal F−F coupling constant of the α-CF_2 resonances determined at 20 °C was held constant for simulation of the high-temperature spectra. The rate constants were obtained via the best fit between the experimental and calculated spectra. The Eyring eq 1 was used to obtain $\Delta G^{\ddagger}$, $\Delta H^{\ddagger}$, and $\Delta S^{\ddagger}$. The plot of $\ln(k/T)$ vs $1/T$ shows good linearity, with r^2 = 0.9956 (Figure 1B). The following activation parameters were derived: $\Delta G^{\ddagger}$ = 14.99(5) kcal/mol, $\Delta H^{\ddagger}$ = 12.37(2) kcal/mol, and $\Delta S^{\ddagger}$ = −0.09(1) kcal/mol K.

$$\ln(k/T) = \ln(k_B/h) + \Delta S^{\ddagger}/R - \Delta H^{\ddagger}/RT \qquad (1)$$

The ^{19}F and ^{1}H NMR spectra of **isoDFH-3T** at various temperatures are more complex (Figure S2) since this system can exist in solution as a mixture of diastereoisomeric rotamers (e.g., planar **A**−**C**, considering only two 180° inter-ring torsions). Therefore, multiple sets of resonances are possible for both fluorocarbon chains and aromatic protons. Indeed, the ^{19}F NMR spectrum of **isoDFH-3T** at 25 °C exhibits multiple sets of resonances for the perfluorohexyl chains, one of which dominates over the entire temperature range investigated (−70 to +100 °C). This major set of signals exhibits equivalent resonances for the α-CF_2 groups, indicating that it is associated with one of the planar symmetric rotamers or more likely with a mixture of conformers in fast interconversion. On the other hand, the minority patterns present in the room- and low-temperature spectra exhibit splitting of the α-CF_2 signals, demonstrating that they are associated with two chiral nonplanar structures. As the temperature is increased, these peaks broaden and eventually collapse in the temperature range +(60−90) °C. At +100 °C, the R^F chains exhibit a single set of resonances. However, a clear coalescence pattern is not observed, probably because of the relative low concentration of these species with respect to the major component(s), and therefore an accurate determination of the barriers associated with the exchange processes is not possible. However, the range of coalescence temperatures is lower than those for **isoDFH-2T** (100−110 °C), and consequently, the barriers to rotation must be lower. The ^{1}H NMR spectrum of **isoDFH-3T** is consistent with the ^{19}F NMR and also shows evidence of a rotameric mixture.

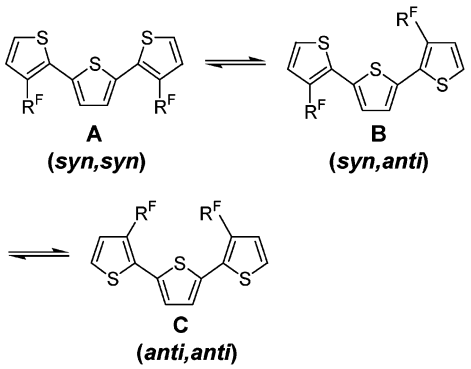

X-ray Crystallography. X-ray structural analysis was performed on four members of the fluorocarbon-substituted series: **DFH-3T**, **DFH-4T**, **isoDFH-5T**, and bisTMS-substituted precursor **25**. Single crystals were prepared by slow cooling of saturated solutions except for **25**, where crystals were obtained by slow sublimation. Important crystallographic data for these compounds are collected in Table S1. The slipped-stacking crystal structures of the end-substituted **DFH-3T** and **DFH-4T** systems exhibit a monoclinic unit cell with eight and four molecules, respectively. Note that all of the unsubstituted oligothiophene αnTs (n = 2−6, 8) crystallize in the monoclinic system as well.[31] The aromatic cores of both structures exhibit an all-*anti*, fully planar geometries, with dihedral angles between the mean plane of the rings <2° (Figure 2A,B). This value compares well to that reported for **α4T** but is much smaller than the 6−9° reported for **α3T**. The perfluorohexyl substituents exhibit a zigzag helical conformation characteristic of fluorocarbon chains[32] and are positioned at ∼140° with respect to the oligothiophene backbone axes in both cases. The molecular packing of **DFH-4T** shares the familiar "herringbone" (HB) motif found in all members of the αnT series, with an angle of 50° between mean planes of adjacent molecules (Figure 2B). Typical HB angles for oligothiophene αnTs (n = 4−6, 8) range between 55 and 70°. The origin of this angle, which is typical of many aromatic hydrocarbons such as *p*-oligophenylenes and acenes, is principally due to intermolecular π-electron repulsion.[31] The minimum interplanar distances between neighboring molecules in **DFH-4T** are found to be 3.02 (C_5−H_7'), 3.52 (C_2−C_4'), 3.54 (C_4−C_7'), and 3.72 Å (S_2−C_6'), comparable to 3.5−3.9 Å in analogous oligothiophenes. The **DFH-3T** solid-state packing appears more complex (Figure 2A), with alternating regions of cofacial π−π stacking (slipped by one thiophene ring) and HB arrangement (with an angle of ∼48°) of dimeric units extending along the *c* axes. The minimal intermolecular distances found in **DFH-3T** are 3.80 (S_1−C_{11}'), 4.05 (S_2−S_1'), and 4.12 Å (S_1−C_{12}') for cofacial dimers, and 3.59 (C_9−C_{15}'), 3.69 (C_{17}−C_{11}'), and 3.71 Å (S_2−C_{14}') for HB dimers.

The crystal structures and packing characteristics of β,β'-disubstituted systems **isoDFH-5T** and **25** are considerably different from those of the end-capped compounds (Figure

(28) It is well-established that the chemical shift of a proton bound to an aromatic system is related to the effective charge on the carbon atom to which the proton is bound. Memory, J. D.; Wilson, N. K. *NMR of Aromatic Compounds*; John Wiley and Sons: New York, 1982.
(29) Hughes, R. P.; Overby, J. S.; Williamson, A.; Lam, K.-C.; Concolino, T. E.; Rheingold, A. L. *Organometallics* **2000**, *19*, 5190.
(30) (a) Di Cesare, N.; Belletete, M.; Leclerc, M.; Durocher, G. J. *Chem. Phys. A* **1999**, *103*, 803. (b) Bongini, A.; Bottoni, A. *J. Phys. Chem. A* **1999**, *103*, 6800. (c) Subramanian, H.; Lagowski, J. B. *Int. J. Quantum Chem.* **1998**, *66*, 229. (d) Salzner, U.; Lagowski, J. B.; Pickup, P. G.; Poirier, R. A. *Synth. Met.* **1998**, *96*, 177. (e) Diaz-Quijada, G. A.; Weinberg, N.; Holdcroft, S.; Pinto, B. M. *J. Phys. Chem. A* **2002**, *106*, 1266. (f) Muguruma, H.; Kobiro, K.; Hotta, S. *Chem. Mater.* **1998**, *10*, 1459. (g) Horne, J. C.; Blanchard, G. J.; LeGoff, E. *J. Am. Chem. Soc.* **1995**, *117*, 9551. (h) Bredas, J.-L.; Heeger, A. J. *Macromolecules* **1990**, *23*, 1150.
(31) For a recent review on oligothiophene crystal structures, see: Fichou, D. *J. Mater. Chem.* **2000**, *10*, 571.
(32) Bunn, C. W.; Howells, E. R. *Nature* **1954**, *174*, 549.

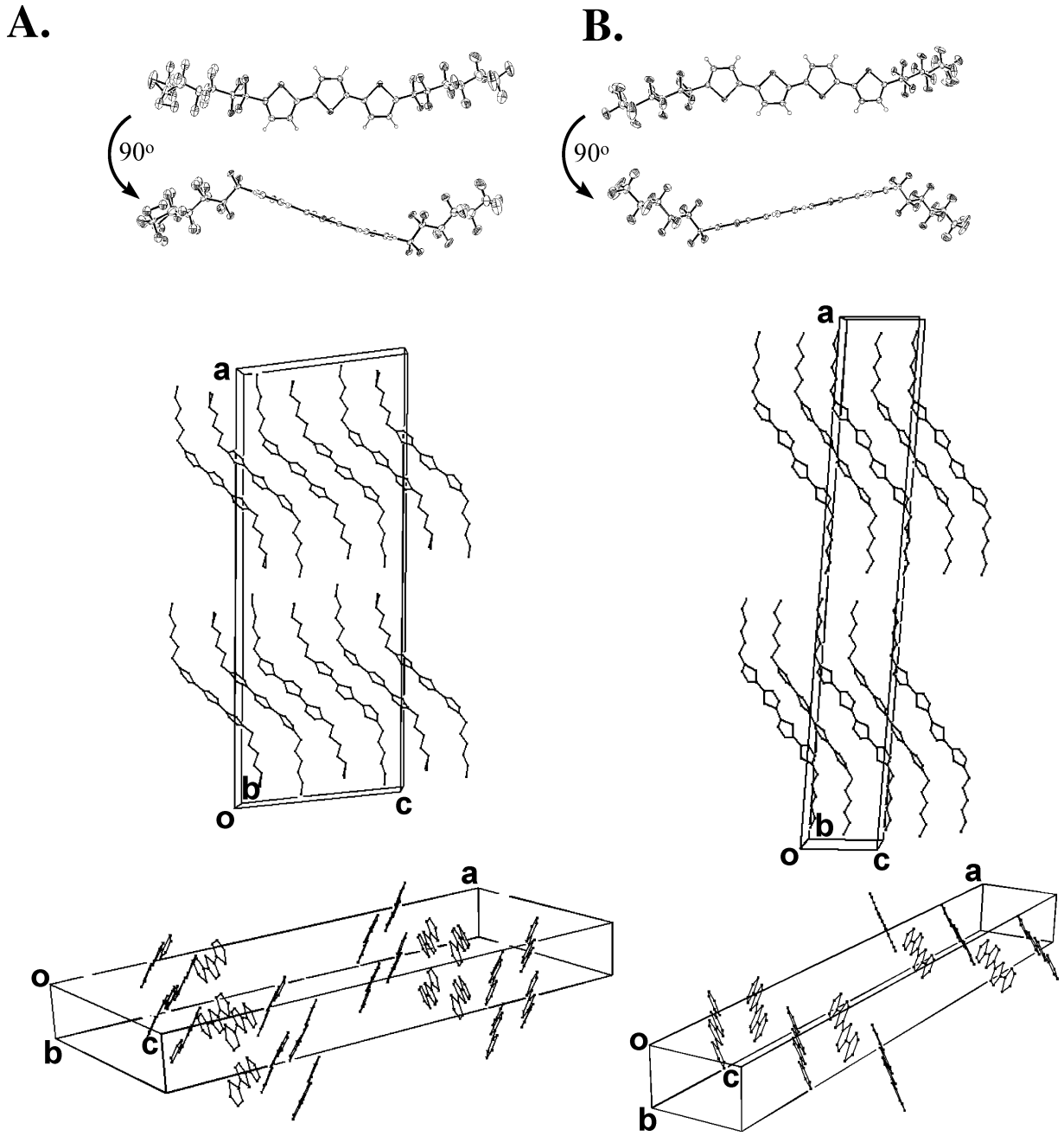

Figure 2. Molecular structure and crystal packing diagram of (A) **DFH-3T** and (B) **DFH-4T**. Fluorine atoms (middle) and fluorocarbon chains (bottom) are removed for clarity.

3A,B). These systems crystallize in a triclinic ($Z = 6$) and monoclinic ($Z = 4$) unit cell, respectively. The effect of $\alpha,\omega \rightarrow \beta,\beta'$ regiochemical substitution on the π-core structure is dramatic with a large torsional angle forced between adjacent thiophene rings compared to the DFH-nTs series. The magnitude of this torsional angle is larger between the two thiophene rings located at the external [31−64° (**isoDFH-5T**); 45.6° (**25**)] versus the internal [1−30° (**isoDFH-5T**); 0.7° (**25**)] core positions. To a lesser degree, this has been observed as well for some β-alkyl-substituted oligothiophenes[33] and is due to steric repulsion between the fluorohexyl chain α-CF_2 group and either the sulfur atom or the C_β-H moiety on the adjacent thiophene ring (vide infra). Compound **25** has one-half an independent molecule in the asymmetric unit, and the core exhibits both *syn* (between outer rings) and *anti* (between inner rings) configurations. The molecular packing in the crystal consists of alternating layers of aromatic TMS and fluorocarbon regions parallel to the *bc* plane (Figure 3B). In each layer, the conjugated backbone forms slipped columnar stacks between the TMS regions along the *b*-axes with a minimum intrastack distance of 3.76 Å (S_2-C_{10}'). The minimum intercolumnar distance is only slightly greater [3.95 Å (S_1-S_2'')] but because of the presence of bulky TMS groups, contacts occur in this direction only at the molecular termini with most of the core π-orbitals not interacting along

(33) (a) Tetramethyl-α4T: Barbarella, G.; Zambianchi, M.; Bongini, A.; Antolini, L. *Adv. Mater*. **1992**, *4*, 282. (b) Dibutyl-α6T: Herrema, J. K.; Wildeman, J.; van Bolhuis, F.; Hadziioannou, G. *Synth. Met.* **1993**, *60*, 239. (c) Dihexyl-α6T: Sato, T.; Fujitsuka, M.; Shiro, M.; Tanaka, K. *Synth. Met.* **1998**, *95*, 143.

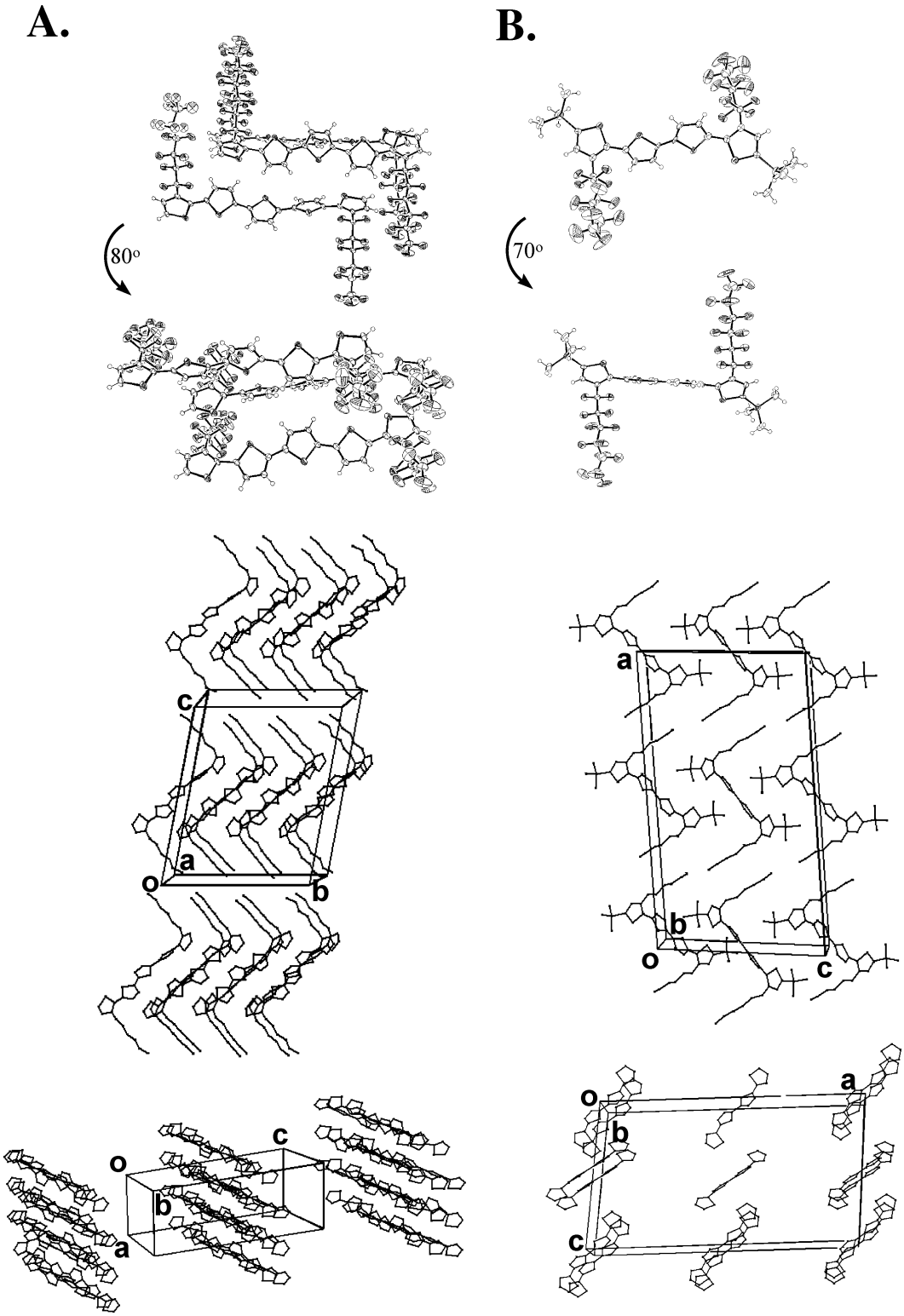

Figure 3. Molecular structure and crystal packing diagram of (A) **isoDFH-5T** and (B) compound **25**. Fluorine atoms (middle) and fluorocarbon chains (bottom) are removed for clarity.

the *c* direction. In the case of **isoDFH-5T**, two of the three independent molecules exhibit a *syn*−*anti*−*anti*−*anti* arrangement (starting from the external ring) and the third, a *syn*−*anti*−*anti*−*syn* conformation. The molecular packing (Figure 3A) shows similarities to those of the other systems, with alternating layers of 5T cores and fluorocarbon chains extending perpendicular to the *c*-axes. Despite the poorly conjugated core, the aromatic thiophene subunits interact strongly, without any apparent order, in both *a* and *b* directions, with close contacts at 4.01 ($C_{18}-S_{10}'$), 3.52 ($C_{10}-C_{43}'$), 3.58 ($C_{10}-C_{44}'$), 3.53 ($C_{47}-S_{13}'$), and 3.87 Å ($C_{39}-S_{11}'$).

Finally, note that, regardless of the differences in molecular structure and packing characteristics, all fluorocarbon-substituted compounds exhibit similar intermolecular separations between

Table 1. Capillary Melting Points, DSC Thermal Transitions, and Volatility Properties of Solid Compounds of Series **1**−**5**

		heating		cooling		
compound	mp (°C)	T_{DSC} (°C)	ΔH (kcal/mol)	T_{DSC} (°C)	ΔH (kcal/mol)	T_{TGA} (°C)[a]
DFH-2T	97	97	11.52	86	11.41	65
DFH-3T	132	131	9.29	124	9.25	91
DFH-4T	213	213	16.33	203	14.94	153
DFH-5T	252	168, 250	0.57, 12.98	244, 152	0.74, 11.44	196
DFH-6T	309	292, 312	9.81, 1.11	292, 284	8.93, 0.72	232
isoDFH-4T	145	158	14.11	139	12.25	119
isoDFH-5T	160	168	11.02	159	10.62	147
isoDFH-6T	217	220	15.42	210	15.84	187
DH-2T	34	34	10.04	10	9.75	84
DH-3T	83	48, 87	3.92, 4.53	78, 31	3.78, 4.18	130
DH-4T	184	88, 186	4.48, 8.15	178, 42	4.41, 7.78	184
DH-5T	254	258	10.29	248	8.78	222
DH-6T	310	300, 308, 314	15.71	309, 300, 295	14.55	270
isoDH-5T	78	77	8.62	48, 44, 37	5.98	186
isoDH-6T	137	147	11.56	130	11.34	277
2T	34	36	4.05	28	3.95	30
3T	95	97	4.67	85	4.57	61
4T	216	221	10.89	210	10.19	144
5T	257	262	10.78	250	10.50	184
6T	309	316	18.45	307	14.97	260

[a] Calculated as the temperature where 2% of the material has sublimed at 10^{-2} Torr.

the oligothiophene and fluorocarbon regions with intercore and interchain distances comparable to the sum of the respective sulfur−sulfur (3.4−3.5 Å), sulfur−carbon (3.4−3.5 Å), carbon−carbon (3.3−3.4 Å), and fluorine−fluorine (3.0−3.1 Å) van der Waals radius sums.

Thermal Properties. The thermal properties of compounds **1**−**5** are reported in Table 1. Within each family, melting points increase with increase in the number of thiophene units. In addition, α,ω-substituted oligomers DFH-nTs (**1**) and DH-nTs (**3**) melt at considerably higher temperatures than the corresponding β,β′-substituted isoDFH-nTs (**2**) and isoDH-nTs (**4**) isomers, as expected considering that lateral substitution of rodlike molecules reduces intermolecular interactions.[13,33] Furthermore, since **2** and **4** are expected to be less planar, the decrease in molecular symmetry is associated with a lowering of the melting point.[34] Particularly interesting is the effect of chemical substitution on the cohesive forces operative in these families of organic materials. Figure 4A plots the melting points of **1**−**5** versus *n* (the number of thiophene rings). In general, the melting points of fluoroalkyl-substituted oligomers are higher than those of the corresponding unsubstituted and alkyl-substituted systems. However, when end-capped systems **1** and **3** are compared to unsubstituted **5**, this plot can be divided into two regions: the first for $n > 4$, where melting points are essentially independent of chemical substitution (H, R^H, R^F), and the second for $n < 4$, where DFH-nT melting points are found to be much higher. This result suggests that in the first region, the intermolecular cohesive forces are dominated by the strong π−π interactions of the extended conjugated cores, whereas the second probably reflects the different specific gravities of F versus H and different chain−chain interactions between alkyl and fluoroalkyl substituents.[20]

The comparative thermal behavior of oligothiophenes **1**−**5** was additionally investigated by DSC and TGA. Although the liquid crystalline properties of polythiophenes have been previously investigated,[35a,b] fewer studies have been reported on oligothiophene LC behavior.[35c−g] Since the relative molecular orientation of the π-conjugated core is a key factor affecting charge transport, the presence of LC phases might be useful to further align the molecular components. For relatively short oligothiophenes, the attachment of alkyl chains to the core is a prerequisite for the appearance of mesophases. Funahashi et al. reported that dialkyl terthiophene derivatives exhibit appreciable charge mobility in their smectic phases, because of the crystal-like ordering of these phases.[35f] Again for terthiophenes, the appearance of liquid crystalline phases strongly depends on the substituents at the α,ω-positions.[35g] The present DSC measurements were performed under nitrogen at heating and cooling rates of 5 °C min^{-1}, and results are collected in Table 1. DSC thermograms for end-substituted systems DFH-nTs (**1**) and DH-nTs (**2**) (Figure S3) reveal that some of these compounds undergo multiple thermal transitions. Upon heating, fluorinated systems **DFH-5T** and **DFH-6T** exhibit the first/second endothermic peaks at 168/250 °C and 292/312 °C, respectively, with a ΔH of +0.57/12.98 and +9.81/1.11 kcal/mol. Polarized optical micrographs indicate that when **DFH-6T** is cooled from the isotropic liquid phase, an anisotropic phase separates from the liquid almost without supercooling. The texture is reminiscent of a smectic liquid crystal (Figure 4B). On the other hand, upon cooling **DFH-5T** below the second transition, the liquid turns into a solid phase that cannot be distinguished by microscopic means as a liquid crystalline phase or a solid phase. In the alkyl-substituted family, multiple thermal transitions are observed for **DH-3T** (48/87 °C, +3.92/4.53 kcal/mol), **DH-4T** (88/186 °C, +4.48/8.15 kcal/mol), and **DH-6T** (300/308/314 °C, +15.71 kcal/mol). Optical micrographs on cooling clearly indicate the presence of a LC mesophase, probably smectic, before solidification for **DH-4T** (Figure 4C), whereas **DH-3T** appears to exhibit a crystal-to-crystal transition before melting. Unfortu-

(34) Brown, R. J. C.; Brown, R. F. C. *J. Chem. Educ.* **2000**, *6*, 724.

(35) (a) Toba, M.; Takeoka, Y.; Rikukawa, M. *Synth. Met.* **2003**, *135*−*136*, 339. (b) Rosu, C.; Manaila-Maximean, D.; Paraskos, A. J. *Mod. Phys. Lett. B* **2002**, *16*, 473. (c) Sharma, S.; Lacey, D.; Wilson, P. *Liq. Cryst.* **2003**, *30*, 461. (d) Liu, P.; Nakano, H.; Shirota, Y. *Liq. Cryst.* **2001**, *28*, 581. (e) Azumi, R.; Götz, G.; Bäuerle, P. *Synth. Met.* **1999**, *101*, 544. (f) Funahashi, M.; Hanna, J. *Appl. Phys. Lett.* **2000**, *76*, 2574. (g) Yamada, T.; Azumi, R.; Tachibana, H.; Sakai, H.; Abe, M.; Bäuerle, P.; Matsumoto, M. *Chem. Lett.* **2001**, *30*, 1022. (h) Ponomarenko, S.; Kirchmeyer, S. *J. Mater. Chem.* **2003**, *13*, 197.

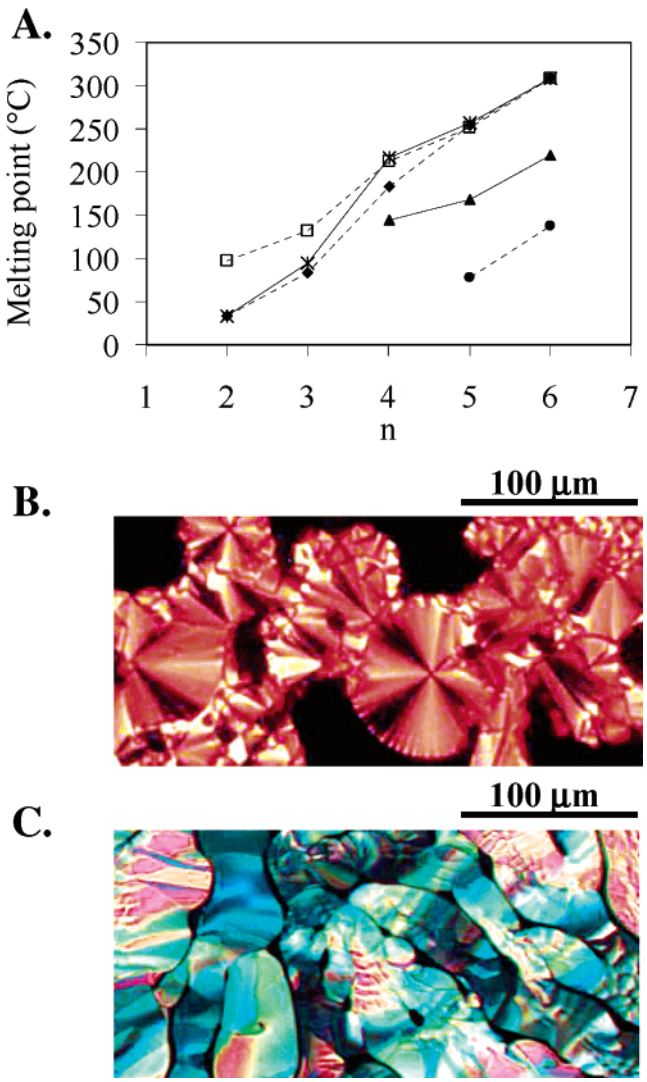

Figure 4. (A) Plot of the melting points of **1**−**5** series [DFH-nTs (□), DH-nTs (◆), isoDFH-nTs (▲), isoDH-nTs (●), αnT (×)] versus the number of thiophene rings (*n*). The lines are a guide to the eye. Polarized micrographs on cooling of (A) **DFH-6T** at 290 °C and (B) **DH-4T** at 174 °C.

nately, the **DH-6T** transitions are above 300 °C and hence not presently accessible to us. However, it is likely that the high-temperature mesophase is liquid crystalline, as suggested by recent results on the corresponding α,ω-didecyl substituted system.[35h] With the exception of **isoDH-5T**, which exhibits three transitions upon cooling, all of the remaining α,ω-substituted systems of series **1** and **3** and the unsubstituted and β,β′-substituted systems **2**, **4**, **5** exhibit a single DSC transition both on heating and cooling (Figure S4). However, the lack of a second peak does not necessarily exclude the presence of mesophases before melting. In fact, it has been observed previously for rigid-rod molecules that the mesophase-to-isotropic transition is frequently not detectable by either optical microscopy or DSC analysis, because of the large difference in the enthalpies associated with the two processes, namely 5−15 kcal/mol for the C-to-M transition and 0.1−0.5 kcal/mol for the M-to-I transition.[36a] This has been demonstrated in the case of **α6T**, where the presence of a mesophase was clearly assigned by XRD.[36b]

The comparative volatility properties of series **1**−**5** (information required for control of film growth) were investigated by low-pressure TGA at 10^{-2} Torr and a temperature ramp of 1.5 °C/min. Most of the literature data regarding semiconducting performance in an FET configuration for unsubstituted nTs (n = 5, 6) and alkyl-substituted DH-nTs (n = 4−6) were obtained on vacuum-deposited films. However, other than our preliminary investigation on **DH-6T**,[23a] no stability or volatility data regarding the sublimation of these classes of materials are available. Table 1 also summarizes the sublimation temperature (T_{TGA}, the temperature where 2% of the material has sublimed) for **1**−**5**. Comparing these values with the corresponding melting points, it can be seen that all fluoroalky-substituted DFH-nTs (**1**) and isoDFH-nT (**2**) derivatives sublime below the melting point by ∼15−80 °C. Interestingly, a similar range is observed for the unsubstituted αnTs. On the other hand, most of the DH-nTs (**3**) and isoDH-nTs (**4**) alkyl derivatives sublime at much higher temperatures and in most cases only above the melting points. Figure S5 shows TGA plots comparing the DFH-nT and DH-nT series, which clearly demonstrate that quantitative, smooth, and residue-free sublimation occurs for all fluorinated derivatives. In contrast, the TGA data of all alkyl-substituted compounds reveal inflection point(s) (Figure S5B), suggesting decomposition processes concomitant with sublimation. A similar trend is observed in the isomeric series isoDFH-nTs and isoDH-nTs (Figure S6). The unsubstituted αnT (**5**) derivatives sublime quantitatively, with the noticeable exception of **α6T**, which leaves ∼6% of residue (Figure S3).

Optical Properties. Optical absorption and fluorescence emission spectra of **1**−**5** were measured both in solution and as thin films to assess the effect of both fluoroalkyl- vs alkyl- and α,ω- vs β,β′-substitutions on oligothiophene absorption and emission maxima ($\lambda_{abs}/\lambda_{em}$) and the (optical) HOMO−LUMO energy gap. Table 2 contains UV−vis/PL data for all compounds in THF solution. As expected, all of these systems are poorly solvatochromic, as verified by the weak shift of λ_{abs} (<10 nm) exhibited by the shortest and longest members of series **1**−**5** (n = 2, 6) in solvents of different polarity (toluene, CH_3CN, dioxane, $CHCl_3$). The solution absorption spectra of **1**−**5** are devoid of any fine structure, whereas splitting of bands due to vibronic coupling can be clearly seen in the fluorescence spectra at room temperature (Figures S7, S8). This coupling is due to planarization of the system upon excitation. The solution ground state is on average twisted, while the excited state is more planar, having greater quinoid character, in agreement with computational studies on oligothiophenes (vide infra). The splitting periodicity as calculated after Gaussian deconvolution (Figure S9) is ∼1400−1500 cm^{-1} and therefore can be attributed to one of the ν(C=C) stretching modes of the oligothiophene core.

The large molar absorption coefficients (ε, Table 2) indicate the dominance in the optical spectra of the allowed conjugated core π → π* transition. As expected, **1**−**5** λ_{abs} values increase throughout the series (n = 2 → 6) for increasing numbers of thiophene units. The magnitude of this shift [$\Delta\lambda_{abs}^{2T\rightarrow 6T} = \lambda_{abs}$ (n = 6) − λ_{abs} (n = 2)] from the 2T to 6T derivatives is 135, 124, and 132 nm for DFH-nTs (**1**), DH-nTs (**3**), and αnTs (**5**), respectively, with the latter value being close to the 130 and 133 nm measured for the unsubstituted oligothiophenes in CH_2-

(36) (a) Johnson, J. F.; Porter, R. S.; Barrall, E. M., II. In *Liquid Crystals 2*; Brown, G. H., Ed.; Gordon and Breach: London, 1969. (b) Destri, S.; Mascherpa, M.; Porzio, W. *Adv. Mater.* **1993**, *5*, 43.

Table 2. Absorption (Maximum of Absorption, λ_{abs} nm, and Extinction Coefficient at λ_{abs}, $\epsilon(M^{-1}\ cm^{-1})$) and Emission Data (Maximum of Fluorescence, λ_{em} (nm), and Quantum Yield, Φ_f) of Compounds **1**−**5** in Dry THF

compound	λ_{max} (ϵ)	λ_f [a]	E_g^{op} [c]	Δ (eV)[b]	Φ_f [c]
DFH-2T	308 (17 500)	369	3.63	0.67	0.03
DFH-3T	360 (28 900)	417, 437*	3.12	0.61	0.26
DFH-4T	398 (39 000)	458*, 489	2.82	0.41	0.50
DFH-5T	421 (40 200)	493*, 525	2.64	0.43	0.73
DFH-6T[d]	443 (53 000)	515*, 547	2.51	0.39	1.00
isoDFH-2T	238 (2600)	308*, 397	4.33	1.18	<0.01
isoDFH-3T	304 (12 700)	429*, 446	3.32	1.19	0.13
isoDFH-4T	356 (25 500)	465*, 489	2.88	0.82	0.26
isoDFH-5T	393 (38 300)	498*,(522)	2.73	0.67	0.51
isoDFH-6T	420 (47 900)	510*, 537	2.60	0.52	0.80
DH-2T	316 (16 800)	377	3.52	0.64	0.03
DH-3T	374 (22 300)	424, 443*	3.04	0.52	0.24
DH-4T	402 (40 000)	463*, 492	2.80	0.41	0.47
DH-5T	426 (42 900)	491*, 523	2.62	0.39	0.55
DH-6T	440 (52 500)[d]	515*, 550	2.54	0.41	0.78
isoDH-2T	269[e] (5400)[f]	314	4.29	0.66	<0.01
isoDH-3T	335 (15 000)	419, 431*	3.14	0.82	0.11
isoDH-4T	377 (28 800)	455*, 480	2.88	0.56	0.38
isoDH-5T	408 (34 700)	484*, 515	2.70	0.48	0.43
isoDH-6T	429 (54 100)	508*, 543	2.58	0.45	0.61
2T	304 (12 800)	363	3.75	0.66	0.01
3T	357 (23 100)	408, 428*	3.14	0.58	0.09
4T	391 (35 000)	450*, 478	2.89	0.42	0.24
5T	418 (46 400)	483*, 513	2.72	0.40	0.39
6T	436 (50 000)[a]	505*, 539	2.61	0.39	0.56

[a] Absolute maximum indicated by asterisk, shoulder in parentheses. [b] $\Delta = \lambda_{em} - \lambda_{abs}$. [c] Measured using 9,10-diphenylanthracene as the standard ($\Phi_f = 0.90$ in cyclohexane). [d] Measure at ~60 °C. ϵ is ±10%. [e] Evaluated at the shoulder. The λ_{max} at 248 nm has been attributed to thiophene ring (Van Hutten, P. F.; Gill, R. E.; Herrema, J. K.; Hadziioannou, G. *J. Phys. Chem.* **1995**, *51*, 3218). [f] At 248 nm.

Cl_2[37a] and dioxane,[37b] respectively. A much larger displacement is observed in both isoDFH-nT (**2**) and isoDH-nT (**4**) families with a $\Delta\lambda_{abs}^{2T\rightarrow 6T}$ of 182 and 160 nm, respectively. This result is due mainly to the short wavelength absorption of 238 and 269 nm for **isoDFH-2T** and **isoDH-2T**, respectively, compared to **α2T** (304 nm). The former value is close to the absorption of thiophene (230 nm in THF),[37c] providing additional evidence that the **isoDFH-2T** core is essentially deconjugated in solution. When comparing the absorption of systems with the same core $[\Delta\lambda_{abs}^{nT}(\mathbf{x} \leftrightarrow \mathbf{y}) = |\lambda_{abs}^{nT}(\boldsymbol{x}) - \lambda_{abs}^{nT}(\boldsymbol{y})|; \boldsymbol{x}, \boldsymbol{y} = \mathbf{1}-\mathbf{4}]$, with the exception of **DFH-6T** and **DH-6T** for which the $\Delta\lambda_{abs}^{6T}(\mathbf{1} \leftrightarrow \mathbf{3})$ value shifts bathochomically by ~3 nm (note that the **DFH-6T** spectrum was recorded at ~60 °C), all of the remaining fluoroalkyl-substituted systems **1** and **2** experience, compared to their alkyl analogues **3** and **4**, a hypsochromic shift (5−31 nm), which can be explained by alkyl group inductive and hyperconjugative effects.[38] In addition, in α,ω-disubstituted nTs **1** and **3**, λ_{abs} values are bathochromically shifted compared to those of the corresponding β,β′-isomers **2** and **4**, respectively, probably because β,β′-disubstitution engenders steric interactions that distort the conjugated π-core from planarity in solution. The extent of this interaction strongly increases when the length of the conjugated core is reduced, since $\Delta\lambda_{abs}^{nT}(\mathbf{1} \leftrightarrow \mathbf{2})$ and $\Delta\lambda_{abs}^{nT}$ ($\mathbf{3} \leftrightarrow \mathbf{4}$) increase on going from the 6T (23 and 11 nm, respectively) to the 2T (70 and 53 nm, respectively) derivatives.

Fluorescence emission spectra were measured in THF by exciting 10^{-5} to 10^{-6} M solutions of **1**−**5** at the corresponding λ_{abs}. The shape of the fluorescence excitation spectra tracks those of absorption. Photoluminescence quantum yields (Φ_f) were determined using 9,10-diphenylanthacene as the standard,[39] and PL data are collected in Table 2. Intrinsically, Φ_f is determined by the relative rate of nonradiative and radiative deactivation. Φ_f values are found to increase quasi-monotonically with the number of thiophene rings. This behavior is similar to that found in the αnT series in dioxane, where Φ_f was found to increase up to six rings and then remain stable or even decrease for longer oligomers.[37b] With the exception of highly twisted oligomers **isoDFH-2T** and **isoDH-2T**, substitution at either α,ω- or β,β′-positions is found to increase the solution quantum yield. Fluorocarbon substitution is found to markedly increase the solution photoluminescence quantum yields in all cases, with the only exception being the **isoDFH-**/**isoDH-4T** couple, with the efficiency of **DFH-6T** approaching unity. This effective modulation of quantum efficiency by chemical substitution must be intimately related to changes in the relative positions of the lowest excited states within the singlet and triplet manifolds and, hence, to changes in the decay rate via efficient nonradiative channels, such as intersystem-crossing processes[40a] due to excimer formation (self-quenching) and intramolecular vibrational or rotational modes.[40] Finally, when the effect of regiochemistry is considered, a lower Φ_f is observed when the substituents are displaced from terminal (DFH-/DH-nTs) to lateral (isoDFH/isoDH-nTs) positions. A similar trend was observed by Demanze et al. for some members of the dicyano-nT series.[41] For conjugated aromatic oligomers and polymers, an additional efficient source of nonradiative deactivation is low frequency, interannular torsional modes, which are dominant for twisted interannular configurations.[40c]

It is interesting to note that when comparing *all* systems with the same conjugation core length *n*, the maximum dispersion in λ_{em} is on average less than that for λ_{abs}, hence $[\Delta\lambda_{em}^{nT}(max) = 63$ (2T), 12 (3T), 10 (4T), 14 (5T), 7 nm (6T)] < $[\Delta\lambda_{abs}^{nT}(max) = 70$ (2T), 56 (3T), 42 (4T), 28 (5T), 23 nm (6T)]. Furthermore, when comparing the $\Delta\lambda_{em}^{nT}/\Delta\lambda_{abs}^{nT}$ of the end-capped series **1** and **3** ($\Delta\lambda_{em}^{nT} = 0-8$ nm/$\Delta\lambda_{abs}^{nT} = 3-14$ nm) with those of the corresponding β,β′-isomers **2** and **4** ($\Delta\lambda_{em}^{nT} = 2-14$ nm/$\Delta\lambda_{abs}^{nT} = 9-31$ nm), it is evident that both $\Delta\lambda_{em}^{nT}/\Delta\lambda_{abs}^{nT}$ values of the latter series are indeed larger than those of the former systems, but $\Delta\lambda_{em}^{nT}$ (**2**/**4**) increases in smaller increments than does the corresponding $\Delta\lambda_{abs}^{nT}$ (**2**/**4**). This apparent anomalous difference in Δλ's can be explained in terms of changes in the nuclear geometries of **1**−**4** upon excitation. In the ground state, the conjugated thienyl cores are largely aromatic, with an average interannular bond order of ~1.[42] Upon excitation to the Franck−Condon excited state, the nuclear

(37) (a) Fichou, D.; Nunzi, J.-M.; Charra, F.; Pfeffer, N. *Mol. Cryst. Liq. Cryst. Sci. Technol., Sect. A* **1994**, *255*, 73. (b) Becker, R. S.; Seixas de Melo, J.; Macanita, A. L.; Elisei, F. *J. Phys. Chem.* **1996**, *100*, 18683. (c) Inoue, S.; Jigami, T.; Nozoe, H.; Aso, Y.; Ogura, F.; Otsubo, T. *Heterocycles* **2000**, *52*, 159.
(38) Di Césare, N.; Belletête, M.; Raymond, F.; Leclerc, M.; Durocher, G. *J. Phys. Chem. A* **1997**, *101*, 776.
(39) Hamai, S.; Hirayama, F. *J. Phys. Chem.* **1983**, *87*, 83.
(40) (a) Beljonne, D.; Cornil, J.; Friend, R. H.; Janssen, R. A. J.; Bredas, J.-L. *J. Am. Chem. Soc.* **1996**, *118*, 6453. (b) Turro, N. J. *Modern Molecular Photochemistry*; University Science Book: Sausalito, CA, 1991. (c) Berlaman, I. B. *Fluorescence Spectra of Aromatic Molecules*; Academic Press: New York, 1971. (d) Pope, M.; Swenberg, C. E. *Electronic Processes in Organic Crystals*; Oxford University Press: New York, 1982.
(41) Demanze, F.; Cornil, J.; Garnier, F.; Horowitz, G.; Valat, P.; Yassar, A.; Lazzaroni, R.; Bredas, J.-L. *J. Phys. Chem. B* **1997**, *101*, 4553.
(42) (a) Xu, B.; Holdcroft, S. *Macromolecules* **1993**, *26*, 4457. (b) Bredas, J.-L.; Themans, B.; Fripiat, J. G.; Andre, J. M.; Chance, R. R. *Phys. Rev.* **1984**, *29*, 6761.

geometry relaxes rapidly (<1 ps)[43] to a more stable configuration, i.e., the equilibrium excited state, with greater quinoid character and an interannular bond order of ~2. Therefore, the first observation indicates that in general the excited states of **1**−**5** having the same *n* differ less electronically than the corresponding ground states, probably because of the rigidification of the excited-state quinoid structure. The second observation suggests that the quinoid form, which has an intrinsically higher degree of coplanarity, is apparently more effective in planarizing the more sterically hindered isoDFH-/isoDH-nTs isomers than the DFH-/DH-nTs. In other words, the excited states of **2** and **4** are still less planar than those of **1** and **3**, but much more so than might be anticipated from ground-state considerations. Similar conclusions were drawn from comparative optical absorption and PL analyses of regioregular (highly conjugated) and regiorandom (highly twisted) 3-hexylpolythiophene.[42b]

The change in conformation to a more planar structure and energy dissipation during the excited-state lifetime are manifest in Stokes shifts, rigorously defined as the energy difference between the 0−0 transitions in absorption and emission.[40d] Since 0−0 transitions are rarely observed in room-temperature solution spectra, it is common procedure to use $\Delta = \lambda_{em} - \lambda_{abs}$ as an indication of the magnitude of the Stokes shift. The observed general trend here is that Δ decreases with increasing *n* and repositioning of substituents from lateral to end positions. Chemical substitution appears to have only a marginal effect. The amplitude of this shift generally tracks the lifetime of the excited state,[40c,d] with longer lifetimes corresponding to increased relative probability of nonradiative decay and correlates with lower PL quantum efficiency. Indeed, these results are in good agreement with the present quantitative Φ_f measurements.

Solution optical gaps (E_g^{op}), defined by the 0−0 transition energies, were estimated from the intercept of the normalized optical absorption and emission spectra, regarded as mirrors of the 0−0 transitions.[40d] The gaps increase with contraction of the core, from 2.51 to 2.62 eV for the 6T derivatives ($n = 6$) to 3.50−4.33 eV for the shortest 2T ($n = 2$) series (Table 2). E_g^{op} values remain in a very narrow range ($\Delta E_g^{op} \leq 0.11$ eV) for oligomers **1**−**5** ($n = 4-6$), and increase for shorter oligomers **1**−**5** ($n = 3$) ($\Delta E_g^{op} \leq 0.25$ eV) and **1**−**5** ($n = 2$) ($\Delta E_g^{op} \leq 0.83$ eV). Figure 5 shows a plot of E_g^{op} versus 1/*n*, where a clear correlation can be discerned. Note that the linear fit of band gaps to 1/*n* for conjugated heterocyclic oligomers has been shown to be only approximate, based on high-quality DFT calculations,[44] but fits extremely well for lengths of 2−6 rings as studied here. The differences between the extrapolated infinite values from 1/*n* are typically on the order of 0.2 eV.[44] A linear increase is observed for all end-capped and unsubstituted DFH-nT, DH-nT, and αnT systems, whereas the plot of more sterically hindered isoDFH-nTs and isoDH-nTs deviates upward for the shortest systems. The projection of the three deviating points on the line (see Figure 5) can be related to the effective conjugation length, which is found to be ~2.5 for **isoDFH-3T** and ~1.5/1.3 thiophene units for **isoDH-2T/isoDFH-2T** vs a theoretical value of 3 and 2, respectively. When comparing systems with the same core length, however, all plots extrapolated to infinite length converge to a value of ~2.1 eV, which compares well with 2.1−2.3 eV found from extrapolation in other oligothiophene classes[45a,b] and 2.1−2.5 eV for soluble regioregular 3-alkylpolythiophenes.[45c]

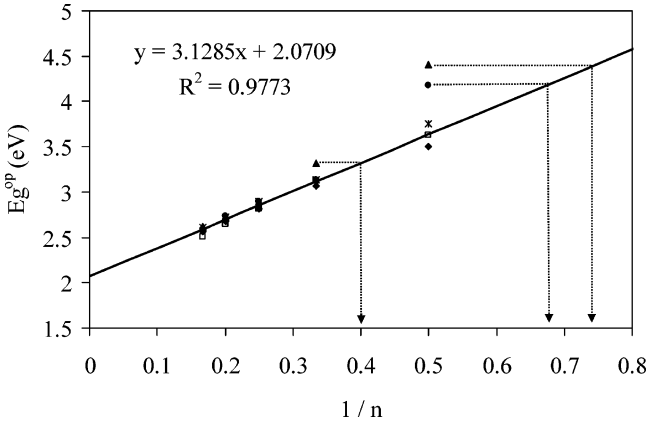

Figure 5. Plot of E_g^{op} versus 1/*n* for molecules **1**−**5**. DFH-nTs (□), DH-nTs (◆), isoDFH-nTs (▲), isoDH-nTs (●), αnT (×). The points corresponding to **isoDFH-3T**, **isoDFH-2T**, and **isoDH-2T** are not included in the linear correlation.

UV−vis/PL data for molecules **1**, **3**, **5** ($n = 3-6$), **2** ($n = 4-6$), and **4** ($n = 5$, 6) as vacuum-deposited thin films are collected in Table S2. The absorption spectra (Figure S8) exhibit characteristic peak(s) at high energy (270−280 nm) found in the spectra of all oligothiophenes and originate from the thiophene ring.[46] The position and shape of the high energy $\pi \rightarrow \pi^*$ transition(s) reflect the interplay of molecular structure, substitution, core length, and solid-state packing. In general within each series, a bathochromic shift of this absorption is observed as core length increases. Unlike the solution behavior, the maxima of alkyl-substituted DH-/isoDH-nTs are shifted to shorter wavelengths compared to those of fluorocarbon DFH-/isoDFH-nTs, while β,β′-substituted isoDFH-/isoDH-nTs exhibit a red shift of the absorption maxima compared to the corresponding end-capped and unsubstituted analogues. As an example, Figure 6 shows comparative UV−vis/PL spectra of molecules **1**−**4** ($n = 5$) in solution and as thin films. Note the similarity between the spectra of α,ω-disubstituted derivatives with the same core length ($n = 4-6$) at long wavelengths, with a strong absorption at 340−380 nm followed by two weaker peaks or shoulders at 410−520 nm. The intense peak at high energies can be attributed to exciton interactions between closed-packed nearest-neighbor molecules. A consequence of the herringbone structures is that the unit cell contains at least two nonequivalent molecular sites. The coupling between the transition dipole of the molecules at nonequivalent sites leads, in the case of a rigid infinite lattice, to the well-known Davydov splitting.[40d,46] When the dipoles are all parallel, the transition between the ground state and the lower crystalline excited state is completely forbidden, thus accounting for the unique intense peak. In analogy with the results of Garnier et al. on **DH-6T**,[46b] the weak absorption at longest wavelengths in the DFH-nT and DH-nT series can be attributed to the 0−0 transition of isolated

(43) Kanner, G. S.; Wei, X.; Hess, B. C.; Chen, L. R.; Vardeny, Z. V. *Phys. Rev. Lett.* **1992**, *68*, 538.
(44) Hutchison, G. R.; Ratner, M. A.; Marks, T. J. *J. Phys. Chem. A* **2002**, *106*, 10596.
(45) (a) Izumi, T.; Kobashi, S.; Takimiya, K.; Aso, Y.; Otsubo, T. *J. Am. Chem Soc.* **2003**, *125*, 5286. (b) Kirschbaum, T.; Briehn, C. A.; Bauerle, P. *J. Chem. Soc., Perkin Trans. 1* **2000**, 1211. (c) Lanzi, M.; Costa-Bizzarri, P.; Della-Casa, C.; Paganin, L.; Fraleoni, A. *Polymer* **2002**, *44*, 535
(46) (a) Garnier, F. *Acc. Chem. Res.* **1999**, *32*, 209. (b) Yassar, A.; Horowitz, G.; Valat, P.; Wintgens, V.; Hmyene, M.; Deloffre, F.; Srivastava, P.; Lang, P.; Garnier, F. *J. Phys. Chem.* **1995**, *99*, 9155.

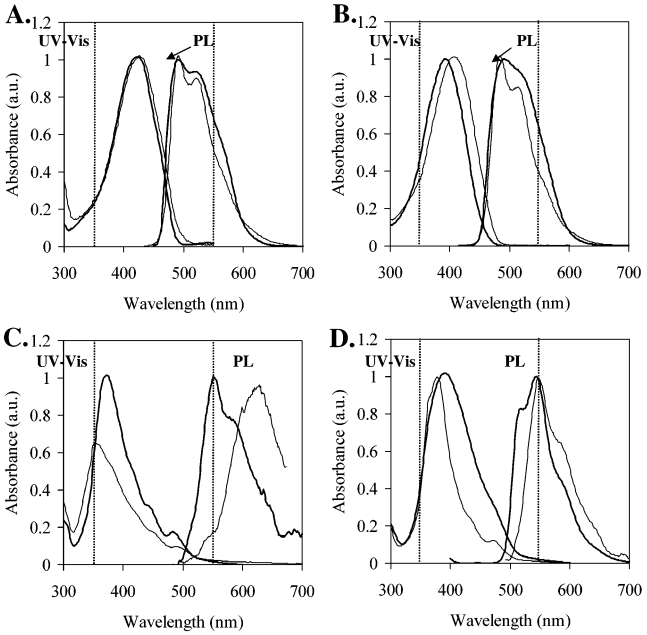

Figure 6. Optical absorption (UV−vis) and emission (PL) spectra of (A) THF solution of **DFH-5T** (thick line) and **DH-5T** (fine line), (B) THF solution of **isoDFH-5T** (thick line) and **isoDH-5T** (fine line), (C) films (50 nm) of **DFH-5T** (thick line) and **DH-5T** (fine line) on glass substrates, and (D) films (50 nm) of **isoDFH-5T** (thick line) and **isoDH-5T** (fine line) on glass substrates. The PL spectra were obtained by exciting the solution at the absorption maximum. Intensities are in arbitrary units.

molecules, located in disordered domains and in grain boundaries, where molecular misalignment would lead to weak intermolecular coupling and no splitting of the excited levels. In fact, the position of this weak absorption rigorously matches the trend observed in solution, with a decrease of the corresponding energy as the oligothiophene core is elongated. The second weak absorption at higher energies has been attributed in the case of **DH-6T** and **α6T** to the corresponding C═C vibronic replica (0.19 eV) on the basis of 13 K spectra.[46b] However, from the present room-temperature data, the second peak lies at an interval of 0.21−0.25 eV, considerably greater than typical energies of aromatic C═C bond stretches.

The shapes of the β,β'-disubstituted isoDFH-/isoDH-nT film absorption spectra resemble those of the corresponding end-capped systems. Particularly informative is the analysis of the absorption maximum energies. As mentioned previously, the position of isoDFH-/isoDH-nT λ_{abs} is red-shifted compared to DFH-/DH-nT values, which cannot be explained assuming a more planar core structure (see the crystal structure discussion above). In addition, λ_{abs} values are blue-shifted compared to the solution values. These two observations suggest significant coupling between molecular transition dipoles in the β,β'-substituted series, generating H-type aggregates. These interactions are weaker than those in the α,ω- families as suggested by smaller blue shifts of λ_{abs} compared to solution values, but much greater than reported for isomeric mixtures of β,β'-dihexyl- and β,β'-didecylsexithiophenes, where the film spectra match those of the isolated molecule (recorded as dilute solutions or in glass matrixes).[46b]

Film photoluminescence spectra were obtained by excitation at λ_{abs}, and data are presented in Table S2. The spectral shapes and maxima strongly depend on molecular structure and substitution, with most plots exhibiting additional peaks and shoulders. The separation between the better-resolved peaks (1300−1500 cm^{-1}) suggests coupling with vibrational modes, probably thiophene C═C stretches along the molecular backbone. On comparing films of identical thickness having molecules with the same conjugation length, the emission intensities of fluorocarbon-substituted DFH-nTs and isoDFH-nTs are up to 3 orders of magnitude greater than those of the corresponding unsubstituted and alkyl-substituted derivatives. Finally, determination of film E_g^{op} parameters is less straightforward because of the multiple absorption and emission transitions. However, reasonable estimation of E_g^{op} can be obtained from the onset of the absorption (at 10% of the maximum). Similar to the solution trends, E_g^{op} values decrease as the core conjugation length increases and are larger for the β,β'-substituted systems. In general, film E_g^{op} values are smaller by 0.1−0.4 eV than the corresponding solution values. A similar trend has been observed for other oligothiophenes.[47]

Electrochemistry. The electrochemical properties of polythiophenes reveal important aspects of chemical and electronic structures, charge injection and storage mechanisms, substituent effects, and physical behavior.[4,48] In this aspect, oligothiophenes have been significantly less investigated.[13,48] Most studies have been performed on limited numbers of compounds, and more importantly, results are frequently compared to measurements performed by other research groups under different conditions of solvent, electrolyte type, and concentration. Although these comparisons are useful and have promoted thiophene-based conductor development, it is difficult to address quantitatively the effects of chemical and regiochemical substitution and oligomer dimensions. This is particularly true for the present systems since the electrochemical effects of σ-only electron-withdrawing and -donating substituents are expected, particularly for larger molecular cores, to be relatively modest.

CV for oligomers **1**−**5** was performed under N_2 in 0.1 THF/$TBAPF_6$ solutions with scanning rates between 60 and 150 mV/s. Most systems exhibit one or two reversible and/or quasi-reversible one-electron oxidation and reduction waves within the range of the solvent and electrolyte window. Figures S10 and S11 show representative voltammograms. When the voltammograms are (quasi)reversible, it is possible to extract formal potentials ($E^{1/2}$) as the midpoints between peak potentials for the forward and reverse scan. Data are summarized in Table 3. In general, the chemical stability of oxidized and reduced **1**−**5** species increases with increasing core length and with substituents in the α,ω-positions. This can be judged from the fact that both $E_1^{1/2}$ and $E_2^{1/2}$ can be measured for almost all of the longer **1**−**5** (n = 5, 6) molecules, whereas among the 2T derivatives (n = 2), $E_1^{1/2}$ could only be determined for **DFH-2T** and **DH-2T** (oxidation) and **DH-2T**, **isoDH-2T**, and **α2T** (reduction). Furthermore, most of the end-capped DFH-nT and DH-nT derivatives exhibit two reversible oxidation and reduction potentials, even for the shorter 3T and 4T cores. In contrast, the isoDFH-nT-, isoDH-nT-, and αnT-charged species of shorter oligomers exhibit less stability upon reduction for the two former systems and upon oxidation for the latter. Interestingly, for isoDFH-nTs, the solutions around the working electrode show

(47) Meng, H.; Zheng, J.; Lovinger, A. J.; Wang, B.-C.; Van Patten, P. G.; Bao, Z. *Chem. Mater.* **2003**, *15*, 1778.
(48) (a) Domagala, W.; Laokowski, M.; Guillerez, S.; Bidan, G. *Electrochim. Acta* **2003**, *48*, 2379. (b) Jagur-Grodzinski, J. *Polym. Adv. Technol.* **2002**, *13*, 615−625. (c) Meerholz, K.; Heinze, J. *Electrochim. Acta* **1996**, *41*, 1839.

Table 3. Anodic (E_a), Cathodic (E_c), and Half-Wave ($E^{1/2}$) Potentials (V) versus SCE of Compounds **1**−**5** in Dry THF under Nitrogen[a]

	oxidation						reduction					
	anodic		cathodic		half		cathodic		anodic		half	
compound	E_{a1}	E_{a2}	E_{c1}	E_{c2}	$E_1^{1/2}$	$E_2^{1/2}$	E_{c1}	E_{c2}	E_{a1}	E_{a2}	$E_1^{1/2}$	$E_2^{1/2}$
DFH-2T[b]	2.14		1.99		**2.06**		−1.22					
DFH-3T[b]	1.61	1.88	1.53	1.76	**1.57**	**1.82**	−1.65	−1.84	−1.54	−1.70	**-1.59**	**−1.77**
DFH-4T[c]	1.41	1.59	1.30	1.50	**1.35**	**1.55**	−1.58	−1.82	−1.49	−1.69	**−1.53**	**−1.75**
DFH-5T	1.22	1.45	1.16	1.32	**1.19**	**1.39**	−1.51	−1.72	−1.37	−1.63	**−1.44**	**−1.67**
DFH-6T	1.11	1.29	1.01	1.15	**1.06**	**1.22**	−1.45	−1.70	−1.38	−1.61	**−1.42**	**−1.65**
isoDFH-2T[b]	2.07						−2.60	−2.89				
isoDFH-3T[c]	2.01						−2.09	−2.23				
isoDFH-4T[c]	1.58	1.94	1.48	1.87	**1.52**	**1.90**	−1.63		−1.54		**−1.58**	
isoDFH-5T	1.41	1.64	1.24	1.46	**1.32**	**1.55**	−1.56					
isoDFH-6T	1.20	1.39	1.14	1.31	**1.17**	**1.35**	-1.60	−1.71	−1.49		**−1.54**	
DH-2T[a]	1.40		1.30		**1.35**		−2.62		−2.42		**−2.52**	
DH-3T[a]	1.15	1.57	1.01	1.46	**1.08**	**1.51**	−2.23		−2.06		**−2.14**	
DH-4T[c]	1.02	1.40	0.90	1.27	**0.96**	**1.32**	−2.01	−2.35	−1.89	−2.24	**−1.95**	**−2.29**
DH-5T	0.96	1.18	0.86	1.08	**0.91**	**1.13**	−1.86	−2.15	−1.76	−2.05	**−1.81**	**−2.10**
DH-6T	0.95	1.15	0.80	1.03	**0.87**	**1.09**	−1.83	−2.05	−1.74	−1.97	**−1.78**	**−2.01**
isoDH-2T[b]			1.02				−3.07		−2.97		**−3.02**	
isoDH-3T[b]	1.26	2.00	0.74	0.88			−2.34		−2.14		**−2.24**	
isoDH-4T[c]	1.13	1.61	1.01		**1.07**		−2.20	−2.45	−2.16	−2.38	**−2.18**	**−2.41**
isoDH-5T	1.07	1.22	0.93	1.11	**1.00**	**1.12**	−1.93	−2.17	−1.79	−2.03	**−1.86**	**−2.10**
isoDH-6T	1.01	1.19	0.88	1.06	**0.94**	**1.12**	−1.88	−2.02	−1.73	−1.93	**−1.81**	**−1.98**
2T[c]			0.77	1.12			-2.60		−2.24		**−2.42**	
3T	1.27		0.80	1.01			−2.14	−2.54	−2.00	−2.40	**−2.07**	**−2.47**
4T	1.40		0.81	1.00			−2.02	−2.33	−1.86	−2.20	**−1.94**	**−2.07**
5T	1.06	1.27	0.95	1.16	**1.01**	**1.22**	−1.83	−2.03	−1.72	−1.93	**−1.78**	**−1.98**
6T	1.02	1.17	0.93	1.08	**0.98**	**1.13**	−1.76	−1.91	−1.66	−1.79	**−1.71**	**−1.86**

[a] Referred to Fc^+/Fc couple in THF (0.50 vs Ag/AgCl; 0.54 vs SCE). Measurements were performed at −10 °C. [b] At −25 °C. [c] At −20 °C.

Scheme 4. Proposed Electrochemical Decomposition Pathways for Radical Anions and Radical Cations of **isoDFH-4T** and **isoDH-4T**

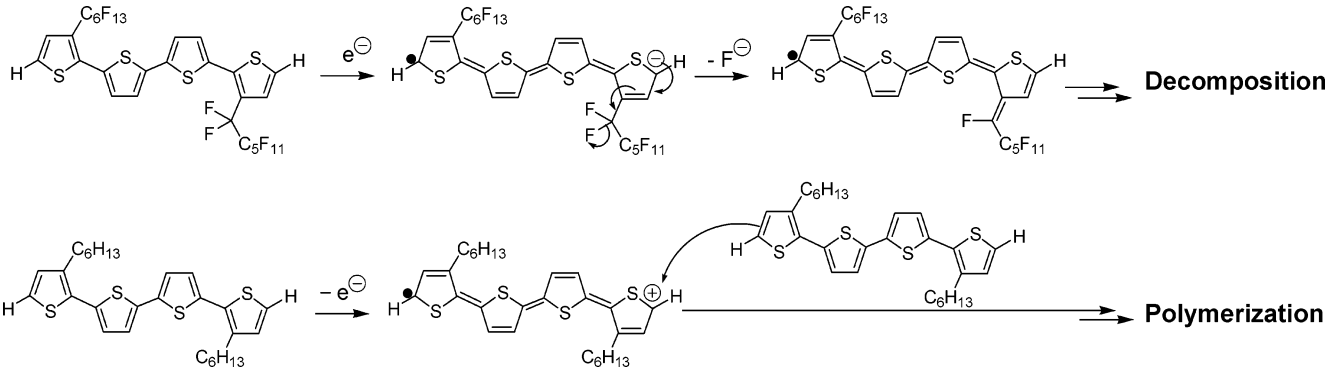

no apparent change after multiple reductive cycles, despite the irreversibility of the process, and repetitive CV plots are essentially superimposable. On the other hand, oxidative cycling of the isoDH-nT and nT solutions produces a green/blue product and film around and/or on the working electrode, and in most cases consecutive forward and reverse scans exhibit increased current during recording and/or growth of additional waves. These results suggest that the origin of the chemical instability upon charging is different for fluoroalkyl and alkyl-unsubstituted oligothiophenes. Reduction of the core (e.g., **isoDFH-4T**) results in preferential negative charge localization over the external thiophene rings, which may promote fluoride elimination from the α-chain position (Scheme 4). The resulting soluble structure will eventually decompose, but not evolve into higher molecular weight species. Indeed, base-promoted dehydrofluorination[49] of 2,2-dihydroperfluoroalkanoic acids, esters, and amides (which can stabilize a negative charge proximate to a $-CF_2R$ group) is known and supports this mechanism. For electron-rich systems (e.g., **isoDH-4T**), the oxidation process generates a radical cation, which can undergo coupling with neutral molecules to produce dimers and, subsequently, larger oligomers and polymers via well-known electropolymerization pathways (Scheme 4).[50] Such a process is prevented in DH-nTs by the alkyl substituents at the α,ω-positions.

Analysis of the half-wave potentials reveals interesting trends within and between these systems, in particular:

(i) Versus unsubstituted oligothiophenes nTs (**5**) with the same core length, the $E_1^{1/2}$ and $E_2^{1/2}$ oxidation and reduction potentials of the corresponding DFH-/isoDFH-nTs (**1**/**2**) are shifted toward larger values [$\Delta E_1^{1/2}$ (**5** → **1**, **2**) = +(0.08−0.52) V, $\Delta E_2^{1/2}$ (**5** → **1**, **2**) = +(0.09−0.70) V], whereas those of DH-/isoDH-nTs (**3**/**4**) are shifted to smaller values [$\Delta E_1^{1/2}$ (**5** → **3**, **4**) = −(0.01−0.44) V, $\Delta E_2^{1/2}$ (**5** → **3**, **4**) = +(0.12−0.29) V]. In addition, the mean magnitude of these shifts is greater for the former than for the latter families. These data

(49) (a) Liu, J.-T.; Lu, H.-J. *J. Fluorine Chem.* **2001**, *111*, 207. (b) Kurykin, M. A.; Vol'pin, I. M.; German, L. S. *J. Fluorine Chem.* **1996**, *80*, 9.

(50) Can, M.; Sevin, F.; Yildiz, A. *Appl. Surf. Sci.* **2003**, *210*, 338. (b) Cha, S.-K. *J. Polym. Sci., Part B: Polym. Phys.* **1997**, *35*, 165. (c) Tourillon, F.; Garnier, F. *J. Electroanal. Chem.* **1982**, *135*, 173.

not only confirm and quantify the expected accepting and donating properties of oligothiophene fluoroalkyl and alkyl substituents but are in agreement with absolute substituent capacities of R^F versus R^H chains (vide infra).

(ii) Within each series, both oxidation and reduction $E_1^{1/2}$ and $E_2^{1/2}$ parameters move to less positive and negative values as the thiophene core size increases. This trend indicates a progressive reduction of the (electrochemical) band gap, in excellent agreement with the aforementioned optical data. Furthermore, $E_1^{1/2}$ displacement is much larger for DFH-/isoDFH-nTs in oxidation [$\Delta E_1^{1/2}$ (2T → 6T) = −(0.35−1.00) V] than in reduction [$\Delta E_1^{1/2}$ (2T → 6T) = −(0.14−0.17) V], whereas for DH-/isoDH-nTs, the shift is larger in reduction [$\Delta E_1^{1/2}$ (2T → 6T) = −(0.37−0.72) V] than in oxidation [$\Delta E E_1^{1/2}$ (2T → 6T) = −(0.35−0.48) V]. These trends reveal a markedly different sensitivity of the energy level positions between fluorocarbon- and alkyl-substituted oligothiophene families with changes in substituent and conjugation length.

(iii) The potential difference between subsequent redox events [$\Delta E^{1/2} = |E_2^{1/2} - E_1^{1/2}|$] decreases as the core length increases [$\Delta E^{1/2}$ = 0.25−0.43 (3Ts), 0.20−0.36 (4Ts), 0.20−0.24 (5Ts), 0.15−0.22 V (6Ts)], consistent with reduction of Coulombic repulsion between excess charges. A similar trend was observed for unsubstituted oligothiophene αnTs and phenylene *p*-nPs series with potentials obtained in CH_2Cl_2 (oxidation) and DMA (reduction).[48c] There are two exceptions: the **isoDH-5T**/**isoDH-6T** couple in oxidation and the entire DFH-nT series in reduction, which may reflect the interplay of core extension (which should stabilize charge as *n* increases) and alkyl steric hindrance or substituent effects (which are attenuated when *n* increases and therefore less effective for injected electron stabilization).

DFT Computation. Theoretical modeling of the electronic structure of conventional oligothiophenes has previously been performed in parallel with experimental work.[13] The parent oligothiophenes have been studied as polythiophene models and as interesting conjugated organic materials in their own right.[44,51] The utility of computational modeling has advanced with the increased accuracy of density functional methods, which can provide accurate estimates of molecular geometries,[52a] including dihedral angles and rotational barriers,[52a−d] dipole moments,[52a,e,f] as well as electronic structure properties such as electron affinity,[52h,g] ionization potential,[52h] and band gaps.[52i,j]

The optimized geometries of compounds **1**−**5** provide molecular lengths for comparison with experimental lengths from crystal structures. Table S3 summarizes molecular core lengths (maximum ring carbon−ring carbon distance along the oligothiophene core) and maximum lengths (the greatest extent of the molecule, including the side chains), illustrating the excellent agreement between computed geometries and experimental crystal structures,[53] particularly for molecular lengths. The dihedral angles found for the computed gas-phase molecular structures are generally greater than those found experimentally in the solid state as might be expected based on solid-state packing effects. Furthermore, as discussed above, with the exception of **isoDFH-2T** and **isoDFH-3T**, all the compounds have low rotational barriers, and several local minima are found in the gas-phase calculations.[52b−d,j]

The lengths of the oligothiophene cores are very similar for various ring substitutions (Figure S12), indicating the typical rigidity of the conjugated cores parallel to the long molecular axes, as well as the common all-*anti* heterocycle conformation prevalent in all oligomers. Each additional thiophene unit is computed to increase the core length by 3.91 Å on average (vs 3.87 Å from the experimental crystal structures),[53] and the perfluorohexyl and hexyl chain lengths are computed to be ∼9.09 and 8.51 Å, respectively, including end group van der Waals radii. Crystal structure data provide similar lengths for the perfluorohexyl and hexyl chains of 9.08 (from **DFH-4T**) and 8.40[54] Å, respectively, probably due to slight conformational differences. IsoDFH-nT **2** members (n = 2−5) are calculated to have slightly bent thiophene cores due to electron−electron repulsion and steric interactions between the perfluoroalkyl chains; however, longer **isoDFH-6T** has sufficient space between the perfluoroalkyl chains to exhibit a less distorted geometry, although still with average interplanar dihedral angles of ∼30°, as shown by the slight deviation in core lengths between the two series at intermediate oligomer lengths (n) (Figure S12). Overall, the perfluoroalkyl-substituted series **1** and **2** have larger gas-phase dihedral angles than their alkyl counterparts (e.g., 12° and 27° vs 7.5° and 0.3° for **DFH-6T**, **isoDFH-6T**, **DH-6T**, and **isoDH-6T**, respectively), perhaps due to greater repulsion between perfluoroalkyl chain fluorine atoms and the π-orbitals in the central oligothiophene.

Similar substituent effects are also observed in computed dipole moment trends for series **1**−**5**, (Table S3). In most cases, these largely symmetric molecules have small dipole moments, computed to be near zero for even thiophene ring numbers and ∼0.6 D for odd thiophene ring numbers, compared to the experimental dipole moment of thiophene, 0.55 D.[55] The perfluoroalkyl chains in molecules **1** (n = 2−6) are essentially planar (and coplanar with the oligothiophene cores) but have staggered spiral conformations due to the fluorine−fluorine repulsions along the chains, and hence, the molecules have dipole moments ranging from 0.54 to 1.88 D (for **DFH-6T** and **DFH-3T,** respectively). Molecules **2** (n = 2−6) and **4** (n = 2−6) also have larger dipole moments since the β,β' substituents are predicted to twist the oligothiophene cores slightly. In some

(51) (a) Ma, J.; Li, S.; Jiang, Y. *Macromolecules* **2002**, *35*, 1109. (b) Springborg, M.; Schmidt, K.; Meider, H.; De Maria, L. *Organic Electronic Materials: Conjugated Polymers and Low Molecular Weight Organic Solids*; Grosso, G., Ed.; Springer: Berlin, 2001; Vol. 41, p 39. (c) Bredas, J.-L.; Cornil, J.; Beljonne, D.; Dos Santos, D. A.; Shuai, Z. *Acc. Chem. Res.* **1999**, *32*, 267. (d) Stafstroem, S.; Bredas, J.-L. *THEOCHEM* **1989**, *57*, 393. (e) Ehrendorfer, C.; Karpfen, A. *J. Phys. Chem.* **1994**, *98*, 7492.

(52) (a) Hehre, W. J. *A Guide to Molecular Mechanics and Quantum Chemical Calculations*; Wavefunction, Inc.: Irvine, CA, 2003. (b) Grein, F. *J. Mol. Struct.: Theochem* **2003**, *624*, 23. (c) Mohamed, A. A. *Int. J. Quantum Chem.* **2000**, *79*, 367. (d) Grein, F. *J. Phys. Chem. A* **2002**, *106*, 3823. (e) Prezhdo, O. V. *Adv. Mater.* **2002**, *14*, 597. (f) Wang, J.; Johnson, B. G.; Boyd, R. J.; Eriksson, L. A. *J. Phys. Chem.* **1996**, *100*, 6317. (g) Rienstra-Kiracofe, J. C.; Tschumper, G. S.; Schaefer, H. F.; Nandi, S.; Ellison, G. B. *Chem. Rev.* **2002**, *102*, 231. (h) Zhan, C. G.; Nichols, J. A.; Dixon, D. A. *J. Phys. Chem. A* **2003**, *107*, 4184. (i) Muscat, J.; Wander, A.; Harrison, N. M. *Chem. Phys. Lett.* **2001**, *342*, 397. (j) Hutchison, G. R.; Facchetti, A.; Ratner, M. A.; Marks, T. J. Unpublished work.

(53) See refs 35a,b and **α2T**: (a) Visser, G. J.; Heeres; G. J.; Wolters, J.; Vos. A. *Acta Crystallogr., Sect. B* **1968**, *24*, 467. (b) Pelletier, M.; Brisse, F. *Acta Crystallogr., Sect. C* **1994**, *50*, 1942. **α4T**: (c) Antolini, L.; Horowitz, G.; Kouki, F.; Garnier, F. *Adv. Mater.* **1998**, *10*, 382. (d) Siegrist, T.; Kloc, C.; Laudise, R, A,; Katz, H. E.; Haddon, R. C. *Adv. Mater.* **1998**, *10*, 379. **α6T**: (e) Horowitz, G.; Bachet, B.; Yassar, A.; Lang, P.; Demanze, F.; Fave, J.-L.; Garnier, F. *Chem. Mater.* **1995**, *7*, 1337.

(54) Destri, S.; Ferro, D. R.; Khotina, I. A.; Farina, A. *Macromol. Chem. Phys.* **1998**, *199*, 1973.

(55) *Handbook of Chemistry and Physics*; CRC Press: Boca Raton, FL, 1995.

cases, such as **isoDFH-3T**, the perfluoroalkyl chains are on the same side of the molecule, giving a large overall dipole moment (3.855 D).

Quantitative analysis of the computed electronic energy levels with respect to experimental data will be discussed in the next section. However, we can anticipate that oligothiophene substitution with *n*-hexyl groups raises both HOMO and LUMO energies vs the unsubstituted analogues (αnT), while *n*-perfluorohexyl groups lower both groups of energy levels (ΔE +0.11 eV for the **DH-6T** HOMO and LUMO vs **α6T**, and −0.41 eV and −0.38 eV for the **DFH-6T** HOMO and LUMO, respectively, vs **α6T**). The electron-withdrawing nature of the perfluoroalkyl substitutents is clearly evident in a plot of the electron density and electrostatic potential. Figure S13 shows that the oligothiophene cores of **DFH-6T** and **isoDFH-6T** have depleted electron density relative to the alkyl-substituted **DH-6T** and **isoDH-6T** molecules. However, the shapes of the HOMOs and LUMOs as well as the topologies of the other frontier MO vary little across all five series (Figure S14).

Discussion

Solid-State Structure. The combination of single-crystal XRD data with thermal analysis and solid-state optical spectroscopies provides fundamental structural insights into the new fluoroalkyl-containing DFH-nTs (**1**) and isoDFH-nTs (**2**) classes and key comparisons with fluorine-free oligothiophenes **3**−**5**.

The solid-state structures and packing characteristics of **1** (n = 3, 4) and **2** (n = 5) are principally a consequence of the geometries and assembling characteristics of the two molecular components, the oligothiophene cores and the fluorocarbon chains, modulated by their relative arrangements. As in other polynuclear aromatics, the first component is an intrinsically flat structure, rich in polarizable π-electron density, which strongly interacts in the π-stacking direction (perpendicular to the molecular long axes) to form 2-D crystals. This property is fundamental to the excellent charge transport characteristics of αnTs (**5**) and should facilitate, according to theoretical modeling, bandlike transport behavior in high-quality single crystals.[56] On the other hand, fluorocarbon chains are insulating, poorly polarizable stiff rods with low intrinsic crystallinity and having the unique characteristic to exhibit, simultaneously, hydrophobic and lipophobic character. *Independent* of the chain arrangement regiochemistry, the first net result of combining these two elements is formation of lamellar-like packing motifs (Figures 2 and 3), with clear local phase segregation between oligothiophene cores and fluorocarbon chains. This is true also for the highly substituted mixed fluorocarbon-TMS structure **25**, where the TMS group "mixes" with the aromatic core, but not with the perfluorohexyl chains (Figure 3B). Similar phase segregation has been proposed for DH-nTs (n = 4,[57a] 6[57b]) based on film XRD analysis, but has never been confirmed with single-crystal data. On the other hand, the crystal structures of several β,β'-dialkyl-substituted oligothiophenes frequently exhibit mixing of hydrocarbon and thiophene fragments,[58] which is not observed in the present fluoroalkyl systems.

When comparing fluoroalkyl series **1** and **2** with alkyl-substituted series **3** and **4**, the positioning of the fluorocarbon chains appears to influence molecular geometry most, in particular the core planarity and conjugation, rather than the overall supramolecular organization. To our knowledge, the only crystal structure reported for an α,ω-dialkyl-substituted oligothiophene is that of α,ω-dimethylquaterthiophene **31**. Comparison of **DFH-4T** and quaterthiophene derivative **25** (and **isoDFH-5T**) with **31** and β,β'-dialkylquaterthiophenes **32** clearly indicates that the **α4T** core geometry is retained for end-capped systems. Minimal differences in core metrical parameters are observed. On the other hand, β,β-disubstituted fluorocarbon derivatives exhibit much greater inter-ring torsional angles compared to **32**, where in the case of **32b** and **c**, the heterocyclic rings are essentially coplanar. These trends are also observed in the aforementioned computed gas-phase geometries.

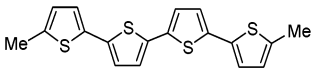

31

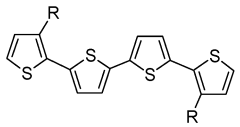

32 : a (R = *n*-C_3H_7)
: b (R = *n*-C_6H_{13}) = **isoDH-4T**
: c (R = *n*-$C_{12}H_{25}$)

From the combined XRD and thermal and optical analyses, the above observations can be extended to the other members of both series. That the melting points of the longer unsubstituted αnTs ($n \geq 4$) are almost identical to those of the corresponding DFH-nTs and DH-nTs is clear evidence that intermolecular forces are dominated by *interactions between the essentially flat cores*. When the core length is reduced, the $\pi-\pi$ stacking forces decrease and interactions among the chains prevail, with the difference between the melting points of **DFH-2T** (97 °C) and **DH-2T** (34 °C) reflecting the characteristics of $C_{12}F_{26}$ (mp = 67 °C) and $C_{12}H_{26}$ (mp = −9.5 °C), respectively. Note that the extrapolated values for $n \rightarrow 0$ (considering a linear regression of melting point versus n) of −17 °C and −116 °C for **1** and **3**, respectively, are much lower than the experimental values obtained for $n = 0$. Such behavior has been also observed for fluorocarbon-substituted benzenes [$F(CF_2)_nC_6H_4(CF_2)_nF$] where melting points are lower than those for the corresponding perfluoroalkanes $F(CF_2)_{2n}F$ and explained by considering that the small aromatic units act as defects in the fluorocarbon lattice.[59] Similar conclusions can be drawn here. For the β,β'-disubstituted series **2** and **4**, lower melting points compared to **1** and **3**, respectively, indicate overall a smaller degree of intermolecular interaction. However, the melting points of fluorocarbon derivatives **2** significantly exceed those of alkyl-substituted compounds **4** (Table 1). This result at first appears

(56) Cornil, J.; Beljonne, D.; Calbert, J.-P.; Bredas, J.-L. *Adv. Mater.* **2001**, *13*, 1053.
(57) (a) Katz, H. E.; Laquindanum, J. G.; Lovinger, A. J. *Chem. Mater.* **1998**, *10*, 633. (b) Garnier, F.; Yassar, A.; Hajlaoui, R.; Horowitz, G.; Deloffre, F.; Servet, B.; Ries, S.; Alnot, P. *J. Am. Chem. Soc*. **1993**, *115*, 8716.
(58) (a) For 3,3‴-didodecyl-α4T, 3,3‴-dihexyl-α4T, and 3,3‴-dipropyl-α4T, see: Azumi, R.; Gotz, G.; Debaerdemaeker, T.; Bauerle, P. *Chem.−Eur. J.* **2000**, *6*, 735. (b) For 3′,4″-didecyl-α4T, see: Wang, S.; Brisse, F.; Belanger-Gariepy, F.; Donat-Bouillud, A.; Leclerc M. *Acta Crystallogr., Sect. C* **1998**, *54*, 553. (c) For 3,3″-dimethyl-α3T, see: Chaloner, P. A.; Gunatunga, S. R.; Hitchcock, P. B. *J. Chem. Soc., Perkin Trans. 2* **1997**, 1597. (d) For 5,5‴″-bis(trimethylsilyl)-4′,3‴″-dioctyl-α6T and 4′,3‴″-di-*n*-butyl-α6T, see: Herrema, J. K.; Wildeman, J.; van Bolhuis, F.; Hadziioannou G. *Synth. Met.* **1993**, *60*, 239.
(59) Schulte, A.; Hallmark, V. M.; Twieg, R.; Song, K.; Rabolt, J. F. *Macromolecules* **1991**, *24*, 3901.

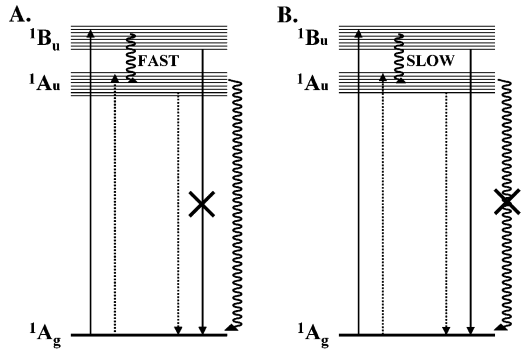

Figure 7. Energy diagram for excitations in films of (A) alkyl- and (B) fluorocarbon-substituted oligothiophenes. Allowed (solid lines) and forbidden (broken lines) optical transitions and nonradiative (wavy lines) decay processes are shown.

to contradict the molecular structures of fluorocarbon systems **2** (and **25)**, where a lower degree of core coplanarity is found, which should correspond to weaker core−core interactions and therefore more facile melting. However, if molecular packing alone is considered, the efficient phase segregation promoted by the fluorocarbon substituents forces the aromatic regions to interact more strongly than would be expected from molecular structures alone. Indeed, the minimum core−core distance in **isoDFH-5T** (3.52 Å) is similar to those in **DFH-4T** (3.52 Å) and **α4T** (3.53[53c]−3.54[53d] Å), but significantly less than that found in planar **isoDH-4T** (**36b**) (3.62 Å).

Additional evidence for comparable intercore interactions is provided by thin-film optical absorption and emission. The similarities between the absorption spectra of **1** and **2** with those of **3** and **4** suggest effective coupling between molecular transition dipoles in the condensed state. The spectral features can be interpreted within the framework of Frenkel molecular excitation theory, which predicts formation of excitonic features associated with Davydov splitting.[46e] The consequences are that the upper 1^1B_u level is accessible by the optical selection rules, whereas the lowest excited level (1^1A_u) becomes forbidden or only weakly allowed. Thus, optical transitions between the ground and the lowest excited state are expected to be very weak both in absorption and emission. This behavior appears to be general for conjugated systems forming H-type aggregates and is observed here for both alkyl-substituted and unsubstituted oligomers **3**−**5**, in which intense absorption is followed by ultrafast relaxation of the upper excited states to the lower excited state, from which almost no fluorescence can be observed (Figure 7). A well-studied example of this behavior is **α6T**, where polycrystalline films deposited at high temperature exhibit photoluminescence quantum yields $\sim 10^{-3}$. On the other hand, we find that all members of fluorocarbon series **1** and **2** exhibit very high solid-state fluorescence yields, which appear at first to contradict the large intermolecular coupling suggested by the λ_{abs} blue shifts and the shapes of the optical absorption profiles. Since the film optical absorption spectra of **1** and **2** are almost superimposable upon the corresponding spectra of **3** and **4**, respectively, the nature of this electronic transition and the electronic states involved must be similar. Furthermore, in addition to different emissive efficiencies, the emission spectra of **1** and **3** appear substantially different in line shape compared to those of **2** and **4**, respectively (Figure S8), suggesting that emission takes place from different excitonic levels. Moreover, $(\lambda_{em})_{max}$ values of fluorocarbon-substituted nTs **1** and **2** are blue-shifted vs **3** and **4**, demonstrating that the emitting excited state of the former systems lies 0.2−0.4 eV (1600−3200 cm^{-1}) *above* that of the corresponding alkyl-substituted systems with the same core length. Although the extent of the Davydov splitting (W_D) in unsubstituted dnT oligothiophenes is still under debate,[60a] recent theoretical and experimental investigations suggest a value of 0.8−1.2 eV,[60a,b] although much smaller numbers have also been reported.[60a] Also, assuming that the W_D's of **1**−**4** are similar to those of the corresponding αnTs, the energy separation between emitting states of **1**/**2** and **3**/**4** is expected to be lower than the W_D values as the result of the mixing of excitonic transitions with different bandwidths between upper and lower Davydov excitonic states. However, the energetic similarities between these parameters and the combined observations of high emission energies and high fluorescence efficiencies for **1** and **2** suggest that emission in the fluorocarbon-substituted nTs takes place from a high-energy optically allowed excited state (Figure 7). A possible explanation is that fluorocarbon chains prevent the fast decay of the ^1B_u to the lower ^1A_u state. We are currently investigating this aspect both theoretically and experimentally.[52j] However, the unprecedented possibility of achieving highly organized oligothiophene supramolecular assemblies with excellent luminescence properties *opens the possibility for new applications and device fabrication strategies*.

Solution Structures and Conformational Analysis. Molecular conformations in π-conjugated systems result from a balance between two major opposing effects: steric forces (favoring $\theta = 90°$, clinical conformations) and π-delocalization forces (favoring $\theta = 0°$, *syn* conformations; or $\theta = 180°$, *anti* conformations). If internal rotation is not greatly hindered, equilibrium conformation(s) in solution may be significantly different from those in the solid state. Many factors may determine the conformational solution phase distribution for oligothiophenes, including molecular structure (core substitution and length), solution temperature and concentration, and solvent polarity.

Useful insights into the "intrinsic" molecular structures of oligothiophenes **1**−**5** can be obtained from solution UV−vis/PL data. Since these measurements were obtained at very low concentrations ($<10^{-5}$) with a solvent of low to mid-dielectric constant (THF, $\epsilon = 7.6$), the influence of molecular aggregation (intermolecular interactions) and differences in molecular dipole moments (highly polar solvents can preferentially stabilize conformations with larger dipole moments) should be minimized.[61] Furthermore, with the exception of **DFH-6T**, the spectra of all compounds were recorded at room temperature. Therefore, differences in spectral features can be ascribed principally to the effects of chemical and regiochemical substitution.

The similarity between the solution optical absorption spectra of **1**−**5** (with the exception described below) having the same core length (Table 2) and the linearity of the plot of the optical gap vs 1/*n* (Figure 5) are strong evidence that conjugation among the core thiophene rings is very similar. Therefore, to a first approximation, the average conformation in solution, which results from free rotation about all inter-ring C−C bonds, is

(60) (a) Sun, H.; Zhao, Z.; Spano, F. C.; Beljonne, D.; Cornil, J.; Shuai, Z.; Bredas, J.-L. *Adv. Mater.* **2003**, *15*, 818. (b) Kouki, F.; Spearman, P.; Valat, P.; Horowitz, G.; Garnier, F. *J. Chem. Phys.* **2000**, *113*, 385.
(61) Hernandez, V.; Lopez Navarrete, T. J. *J. Phys. Chem.* **1994**, *101*, 1369.

essentially identical for all oligothiophenes, independent of substituent effects (identity and position), and core conjugation length. However, the shorter β,β'-disubstituted systems **isoDH-2T** and isoDFH-nTs ($n = 2, 3$), which exhibit shorter λ_{abs} and deviate considerably from the plot of Figure 5, clearly depart from this picture. These data demonstrate a smaller degree of overlap between thiophene π-orbitals, and therefore the averaged core conformation(s) of the latter systems are less planar than those of the former.

To shed more light on the conformational mobility of **1**−**5** and how it affects the corresponding substituted polythiophene structures, optical data were combined with NMR spectroscopy and DFT computation. With the exception of **isoDFH-2T** and **isoDFH-3T**, the ^{1}H and ^{19}F NMR spectra of all systems including **isoDH-2T** exhibit a single set of resonances, consistent with the presence of single species or mixtures of conformers in rapid interconversion. On the basis of the DFT results for **1**−**5** and previous experimental and theoretical work on (oligo, poly)thiophenes,[30a−e,52a−d,62] the second scenario reflects the situation in solution, where many of the envisioned conformers have comparable energies, and the barriers to their interconversion are very small (<1−2 kcal/mol). In contrast, NMR analysis of **isoDFH-2T** and **isoDFH-3T** indicates the presence of rotamers that interconvert much more slowly. The barrier to interconversion of **isoDFH-2T** rotamers is ∼12.4 kcal/mol. This rotational barrier observed by VT NMR compares favorably with the rotational energy profile calculated for **isoDFH-2T** (Figure 8A), which exhibits a single significant energetic minimum at an inter-ring dihedral angle of 117.2° and a barrier of 25.1 kcal/mol to reach the 180° planar *anti* conformation. Since the computational method does not account for geometric relaxation during rotation, this value can be taken as an upper limit, especially since repulsion between the sulfur and perfluoroalkyl chains makes the greatest contribution to the rotational barrier. Furthermore, the modeling clearly shows that rotations that eclipse the two perfluoroalkyls are unfavorable, with an estimated barrier of 1592 kcal/mol for the 0° planar *syn* conformation. Therefore, these data indicate that, contrary to **α2T**[51e] and **isoDH-2T** (vide infra), *syn* conformations are not populated for **isoDFH-2T** in solution, and the *R*/*S* interconversion follows a well-defined pathway.

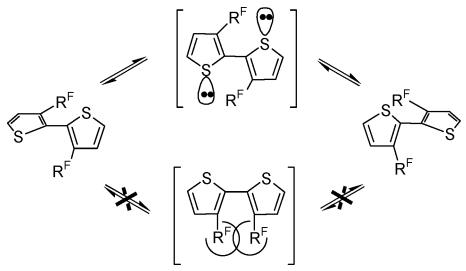

The interconversion barrier (Figure 8A) for the corresponding *R* and *S* rotamers of **isoDH-2T** is calculated to be only 0.7 kcal/mol (at 165°, *anti* conformation), and the barrier to alkyl group crossing in the 0° planar *syn* conformation, 42.0 kcal/mol. The computation indicates that both *syn* and *anti* conformers have similar energies and are therefore present in solution. Their

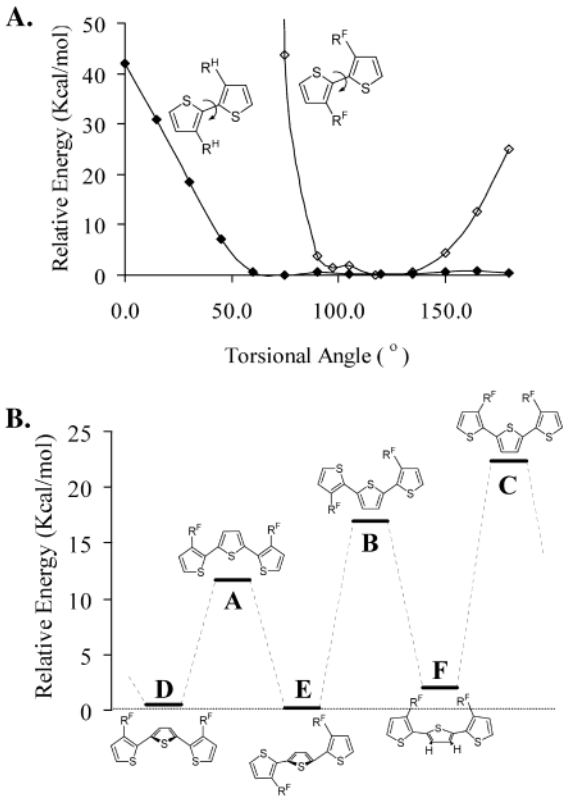

Figure 8. (A) Computed rotational barriers for **isoDFH-2T** (open symbols) and **isoDH-2T** (filled symbols) and (B) computed energy profile for the planar *syn*,*syn* (A), *syn*,*anti* (B), and *anti*,*anti* (C) conformations, and *syn*,*syn* (D), *syn*,*anti* (E), and *anti*,*anti* (F) local minima of **isoDFH-3T**.

interconversion barrier is computed to be ∼0.6 kcal/mol. These modest barriers are in agreement with the averaged conformational structures observed by ^{1}H NMR (vide supra). Finally, as far as **isoDFH-3T** is concerned, we have not computed the entire 2-D torsional potential energy surface, since adequate treatment of the rotation around both inter-ring bonds would require a very large computational effort. Instead, Figure 8B shows three computed *syn*−*syn* (**D**), *syn*−*anti* (**E**), and *anti*−*anti* (**F**) local minima obtained from relaxation of the three planar (**A**−**C**) diastereomeric rotamers (for the computed structures, see Figure S15). The latter conformations can be assumed to be upper limits to energy barriers for interconversions between the various minima (Figure 8B). These computations provide an estimate for A ⇌ B ⇌ C interconversion of 10−20 kcal/mol, although alternative low-energy pathways cannot be ruled out completely. Despite the approximations involved, these data suggest two important conclusions, both supported by the NMR data. First, many different nonplanar rotamers of **isoDFH-3T** are populated in solution. Although the energy differences between these minima are not large, from composition-equilibrium free-energy relationships, the corresponding relative populations are significantly affected.[63] Therefore, energy differences of a few kilocalories per mole correspond to large differences in conformer distributions. Second, the interconversion barriers for **isoDFH-3T** are estimated to be lower than for **isoDFH-2T**, but much larger than those of the other isoDH/isoDFH-nTs.

From these results, important insights into the design and structure of fluorocarbon-substituted polythiophenes (3-perfluo-

(62) In particular, the density functional methods appear to overestimate the stability of planar π-systems, resulting in an underestimation of dihedral angles and an overestimate of the rotational barrier. See refs 51e and 52.

(63) Eliel, E. L. *Stereochemistry of Carbon Compounds*; McGraw-Hill: New York, 1962.

Table 4. Electrochemical, Optical, and Computed HOMO−LUMO Energy Gap (E_g) and Absolute HOMO and LUMO Energies for Compounds **1**−**5**

	energy (eV)				energy gap (eV)		
	experimental[a]		theoretical				
compound	HOMO	LUMO	HOMO	LUMO	E_g^{CV} [b]	E_g^{op} [c]	E_g^{th} [d]
DFH-2T	−6.90	(−3.27)	−6.42	−2.26		3.63	4.16
DFH-3T	−6.41	−3.25	−5.88	−2.39	3.16	3.12	3.48
DFH-4T	−6.19	−3.31	−5.58	−2.39	2.88	2.82	3.18
DFH-5T	−6.03	−3.40	−5.36	−2.50	2.63	2.64	2.86
DFH-6T	−5.90	−3.42	−5.20	−2.56	2.48	2.51	2.64
isoDFH-2T			−6.58	−1.80		4.33	4.79
isoDFH-3T			−5.88	−2.15		3.32	3.73
isoDFH-4T	−6.36	−3.26	−5.58	−2.15	3.10	2.88	3.43
isoDFH-5T	−6.16	(−3.43)	−5.33	−2.29		2.73	3.05
isoDFH-6T	−6.01	−3.30	−5.17	−2.29	2.71	2.60	2.88
DH-2T	−6.19	−2.32	−5.14	−1.01	3.87	3.52	4.14
DH-3T	−5.92	−2.70	−4.87	−1.52	3.22	3.04	3.35
DH-4T	−5.80	−2.89	−4.76	−1.80	2.91	2.80	2.97
DH-5T	−5.75	−3.03	−4.71	−1.96	2.72	2.62	2.75
DH-6T	−5.71	−3.06	−4.68	−2.07	2.65	2.54	2.61
isoDH-2T	(−6.00)	−1.82	−5.17	−0.95		4.29	4.22
isoDH-3T	(−5.74)	−2.60	−4.90	−1.47		3.14	3.43
isoDH-4T	−5.91	−2.66	−4.90	−1.69	3.25	2.88	3.21
isoDH-5T	−5.84	−2.98	−4.82	−1.88	2.86	2.70	2.94
isoDH-6T	−5.78	−3.03	−4.65	−2.07	2.75	2.58	2.58
2T	(−6.22)	−2.42	−5.47	−1.25		3.75	4.22
3T	(−5.91)	−2.77	−5.14	−1.69		3.14	3.46
4T	(−5.79)	−2.90	−4.95	−1.93		2.89	3.02
5T	−5.85	−3.06	−4.87	−2.10	2.79	2.72	2.78
6T	−5.82	−3.13	−4.79	−2.18	2.69	2.61	2.61

[a] The values reported in parentheses are estimated using the optical gap. [b] From electrochemical data: $E_g^{CV} = E_1^{1/2}$ (Ox) − $E_1^{1/2}$ (Red). [c] From optical data. [d] From DFT computations.

roalkyl-pTs) can be drawn. In particular, note that 3-perfluoroalkyl-pTs will have significantly greater steric constraints than the corresponding alkyl-substituted polymers (3-alkyl-pTs). It is known that the regioregular head-to-tail (H−T) 3-alkyl-pTs are a class of highly conjugated (semi)conducting polymers. The corresponding regiorandom or regioregular head-to-head (H−H) systems are less planar and ordered but still exhibit substantial π-delocalization.[4] Our results demonstrate that both regiorandom and H−H 3-perfluoroalkyl-pTs *should not form a class of highly conjugated polymers*. To achieve some degree of core conjugation in the former systems requires the fluorinated substituents be separated by at least 2−3 thiophene rings.

Energy Level Correlations. Important information on the molecular HOMO and LUMO energy levels can be drawn from an accurate analysis of electrochemical and optical data supplemented by theoretical calculations. Table 4 collects electrochemical, optical, and computed energy gaps for classes **1**−**5**. The first important observation is the excellent agreement between solution E_g^{CV} and E_g^{op} data, with differences of ∼0.1−0.2 eV for almost all compounds. Since these are two independently derived measurements, the good agreement supports the accuracy of the results. Table 4 also summarizes the experimental and computed HOMO and LUMO energies, calculated from the first oxidation and reduction potentials ($E_1^{1/2}$), respectively.[64] Because of the good agreement between E_g^{CV} and E_g^{op}, HOMO and LUMO energies associated with irreversible oxidative and reductive events are estimated from the corresponding electrochemically derived LUMO and HOMO energies by addition and subtraction of the corresponding optical gaps.

While HOMO and LUMO eigenvalues from DFT methods cannot be formally taken as either ionization potentials or electron affinities,[65a,b] previous work has shown that B3LYP-derived eigenvalues compare favorably with experimental ionization potentials and electron affinities.[52g,h] The present systematic agreement between computed HOMO and LUMO energies and experimental values is shown in Figure S16. The principal disparity between computed and electrochemical HOMO and LUMO values derive from the difference in environments, and previous work has shown that solvation effects such as polarizability and cavity radius can be used to linearly adjust (via a Kamlet−Taft relationship)[65d] computed ionization potentials and electron affinities to compare to electrochemical data.[65c] In particular, the slopes of the linear relations shown in Figure S16 match the behavior predicted from polarizability effects.[65c] However, for the correlations between electrochemical and computed HOMO values in Figure S16B, there is somewhat greater scatter, perhaps because of the greater number of molecules where electrochemical HOMO energies were estimated from the optical gap. Moreover, the magnitudes of the solvation effects appear to be larger for molecules with smaller ionization potentials, although the absolute differences between computed and experimental HOMO energies across the molecular range studied here are small (0.38 eV on average, vs 0.55 eV for the LUMOs). Finally, the energy gaps also exhibit excellent overall agreement between electrochemical and optical data and the computed DFT orbital energies, although the vertical transition energies predicted from theoretical gaps are greater than the E_g^{CV} or E_g^{op} data in Table 4, as expected.[44]

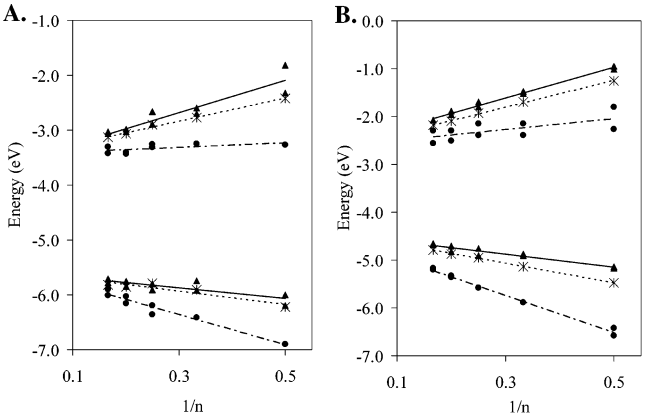

Figure 9. Plots of the (A) experimental and (B) computed molecular orbital energetics of oligothiophene families **1**−**5** studied vs the number of heterocycle rings in the oligomer. DFH-nTs and isoDFH-nTs (●), DH-nTs and isoDH-nTs (▲), αnT (×).

Particularly instructive here are the linear energetic trends revealed by plotting the experimental and computed orbital energies versus 1/*n* (Figure 9). The HOMO and LUMO energy plots of fluorocarbon-substituted **1**/**2** and alkyl-substituted **3**/**4**

(64) The energy level of the normal hydrogen electrode (NHE) is −4.6 eV below the vacuum level (see Bard, A. J.; Faulkner, L. R. *Electrochemical Methods: Fundamentals and Applications*; Wiley: New York, 1984). The oxidation potential of ferrocene is 0.67 V versus the NHE (see Wang, J.-F.; Kawabe, Y.; Shaheen, S. E.; Morrell, M. M.; Jabbour, G. E.; Lee, P. A.; Anderson, J.; Armstrong, N. R.; Kippelen, B.; Mash, E. A.; Peyghambarian, N. *Adv. Mater*. **1998**, *10*, 230). The HOMO/LUMO energies were determined using the Fc calibration against the vacuum energy level. The terms HOMO and LUMO are a convenient short hand since the actual energies correspond to states, not levels.

(65) (a) Godby, R. W.; Schluter, M.; Sham, L. J. *Phys. Rev. B* **1988**, *37*, 10159. (b) Stowasser, R.; Hoffmann, R. *J. Am. Chem. Soc.* **1999**, *121*, 3414. (c) Kamlet, M. J.; Abboud, J. L. M.; Abraham, M. H.; Taft, R. W. *J. Org. Chem.* **1983**, *48*, 2877. (d) Jonsson, M.; Houmam, A.; Jocys, G.; Wayner, D. D. M. *J. Chem. Soc., Perkin Trans. 2* **1999**, 425.

are located below and above those of the unsubstituted oligothiophenes αnTs (**5**), respectively. This result is in agreement with established donating and accepting properties of hexyl and perfluorohexyl substitutents. Furthermore, the slopes (*s*) of these plots (Figure S17) are of particular importance, since they provide quantitative information on substituent effect sensitivity. The Hammet σ-constants for fluorocarbon chains (e.g., CF_3-CF_2 $\sigma_m = 0.47$, $\sigma_p = 0.52$) are greater than those of alkyl substituents (e.g., CH_3CH_2 $\sigma_m = -0.07$, $\sigma_p = 0.15$),[20] meaning not only that the $E_{HOMO/LUMO}$(**1**/**2**) < $E_{HOMO/LUMO}$(**5**) < $E_{HOMO/LUMO}$(**3**/**4**) but also that the progressive diminution in $E_{HOMO/LUMO}$(**1**/**2**) with respect to **5** should be 3−4 times larger than the corresponding increase in $E_{HOMO/LUMO}$(**1**/**2**). The slopes for the HOMOs [$s = -2.74$ (**1**/**2**), -1.22 (**5**), -0.96 (**3**/**4**)] and LUMOs [s = 0.40 (**1**/**2**), -2.10 (**5**), -2.93 (**3**/**4**)] indicate that on average, the relative reduction effect of R^F is ∼1.6, whereas the increment effect of R^H is ∼0.5, in excellent agreement with a straightforward substituent effect model.

Another interesting aspect of these energy diagrams concerns the different sensitivities of the energy levels in **1**−**5** to the core length *n*. For unsubstituted αnTs (**5**), the reduction of the HOMO−LUMO gap on going from $n = 2 \rightarrow 6$ is accompanied by simultaneous, monotonic reduction of E_{LUMO} and increase of E_{HOMO}. The other oligothiophene families behave differently, with E_{LUMO} of fluoroalkyl-substituted systems **1** and **2** being substantially stable across the series and E_{HOMO} being strongly affected. To a lesser degree, the converse is observed for alkyl series **3** and **4**. These trends, nicely reproduced by DFT computation, result from the interplay between intrinsic substituent effects (vide supra), variation in conjugative extension, and the number of substituents per thiophene unit. As a function of core length, substituent effects and substituent density fall with increasing oligomer chain length. Thus, compared to the unsubstituted systems, greater reduction and increment of fluoroalkyl- and alkyl-substituted oligothiophene MO energies are expected for the smaller (2T) vs larger (6T) cores, with the net result being invariant LUMO energies for **1**/**2** and invariant HOMO energies for **3**/**4** across the spectrum of core lengths (Figure 9). Consequently, on going from 6T → 2T derivatives, the energies of the relevant orbitals (LUMOs and HOMOs for **1**/**2** and **3**/**4**, respectively) vary more than in the unsubstituted oligothiophenes. These results suggest that from the molecular viewpoint, the energetics involved in injecting electrons (holes) into LUMO (HOMO) orbitals of **1** and **2** (**3** and **4**) should be rather similar, *independent of the core length*. Therefore, all device processes and performance metrics intimately related to the absolute position of these orbitals should be, in principle, equally manifested by all substituted oligothiophenes.

Conclusions

In this contribution, we describe the synthesis and comparative physicochemical properties of five new oligothiophene classes. The syntheses of end-capped fluorocarbon-substituted DFH-nTs and of novel, isomerically pure β,β'-disubstituted isoDFH/isoDH-nT systems are presented in detail. All of the new compounds have been characterized in depth. Thermal analysis measurements indicate that all of fluorocarbon-substituted systems have excellent thermal stability and volatility. Furthermore, some of these compounds exhibit multiple thermal transitions before melting, with **DFH-6T** clearly exhibiting a smectic LC phase. Optical spectroscopic data indicate that chemical substitution has, in most of the cases, little effect on the optical absorption spectra and HOMO−LUMO gap, which are instead strongly affected by the core conjugation lengths. PL emission spectroscopy demonstrates that all oligothiophenes **1**−**5** are conformationally more rigid in their excited states, as indicated by coupling of the electronic emission transitions to vibrational modes. In addition, the emission quantum efficiencies of DFH/isoDFH-nTs are found to be significantly greater than those of other oligothiophenes. Optical data and VT NMR spectroscopies provide insights into the solution molecular geometries and conformational dynamics. For the first time, the interconversion energy barrier between oligothiophene rotamers has been quantified by dynamic NMR and found to be, in the case of **isoDFH-2T**, ∼10 kcal/mol, much larger than that of the corresponding alkyl-substituted **isoDH-2T**. This result indicates that fluorocarbon chains on an oligothiophene core present greater stereoelectronic impediments to planarization of the polyheterocyclic core.

The crystal structures of key fluorocarbon-substituted oligomers are also analyzed, and evidence shows close $\pi-\pi$ intermolecular interactions between the aromatic cores, whereas the fluorocarbon chains segregate into lamellar structures. From the combined analysis of the thermal and film optical data, these considerations can be extended to other members of the fluoroalkyl families. Surprisingly, despite these strong intermolecular interactions, unprecedented high solid-state optical emission efficiencies are observed in the fluorocarbon-substituted oligothiophene films.

Finally, electrochemical measurements performed under stringent, identical experimental conditions allow straightforward comparison between the redox behaviors of unsubstituted and fluorocarbon- and alkyl-substituted oligothiophenes. Combining the electrochemical and optical data, the energy positions of **1**−**5** HOMOs and LUMOs are estimated. The shift of DFH/isoDFH-nT and DH/isoDH-nT HOMO and LUMO energies with respect αnTs is in quantitative agreement with the expected effects of fluorocarbon and hydrocarbon substituent-derived Hammett σ-parameters. Overall, the **1**−**5** molecular orbital energy trends within each series are determined by a balance between substituent nature and density vs the extension of the aromatic core. The net results from this interplay are frontier MOs where LUMO and HOMO energies are practically independent of conjugation length for fluorocarbon- and alkyl-substituted nTs, respectively. These results are confirmed and explained by density-functional computational modeling, the results of which closely parallel experimental trends.

The above observations and results indicate that the new oligothiophene series **1**−**5** are truly complementary in many aspects of their optoelectronic properties. Indeed, important consequences of these properties directly impact applications as semiconducting materials for organic thin-film transistors, as detailed in a closely related contribution.[22]

Acknowledgment. We thank ONR (N00014-02-1-0909) and the NSF-MRSEC program through the Northwestern Materials Research Center (DMR-0076097) for support of this research. This work was also supported by the NASA Institute for Nanoelectronics and Computing under Award No. NCC 2-3163. We thank Dr. C. Zuccaccia for helpful discussions of the VT NMR experiments.

Supporting Information Available: Synthetic details and film deposition methods. ^{19}F NMR of isoDFH-3T. DSC thermograms and TGA plots of **2**, **4**, and **5**. FT-IR spectra of **2**, **3**, and **4**. UV−vis/PL spectra of **1**−**4** in THF and as thin films. Gaussian deconvolution of DH-6T and DFH-6T spectra. CV plots of selected **1**−**5**. Computed HOMO and LUMO orbitals of **1**−**5** ($n = 6$). Computed planar transition states of isoDFH-3T. CIF and plain text files of DFH-3T, DFH-4T, and isoDFH-5T, **26**. This material is available free of charge via the Internet at http://pubs.acs.org.

JA048988A